Politecnico di Torino

Politecnico di Torino
Department of Applied Science and Technology

Master's Degree in Physics of Complex Systems

Dynamical transitions in the TASEP with local inhomogeneities: mean-field theory

Supervisors:

Prof. Alessandro Pelizzola
Prof. Marco Pretti

Candidate:

Amedeo Di Fede

ACADEMIC YEAR 2025-2026

Abstract

The Totally Asymmetric Simple Exclusion Process (TASEP) has become a paradigmatic model for studying and understanding nonequilibrium systems such as traffic or transport phenomena.

The TASEP with open boundaries can be defined on a one-dimensional lattice of L sites. Once a direction is fixed, particles enter with rate α from the first site, hop throughout the lattice subject to hard-core exclusion and then exit with rate β from the last site.

In this work, through the use of mean-field theory, we investigate the behavior of the TASEP in the presence of local inhomogeneities, or in more detail, in which all hopping rates are uniform (and unitary) apart from a (local) region far from the boundaries in which the hopping rate is smaller, modeling a bottleneck.

Its stationary states and the corresponding phase diagram are presented, the relaxation to stationarity and in particular the dynamical transitions, i.e. transitions in the value of the largest relaxation time, or equivalently the lowest relaxation rate, are discussed as a function of the parameters of the model. All results are obtained through numerical solutions; when possible, analytical results are presented and discussed.

The (mean-field) phase diagram is found to be similar to known results, whereas the relaxation behaviour (which has not previously been investigated) is richer than the picture found in the literature for ordinary TASEP, in particular since it shows dynamical transitions even in the phase separation regime.

Contents

Chapter 1

Introduction

In the field of Statistical Physics, Non-equilibrium Statistical Physics is still an open and active area of research, whereas Equilibrium Statistical Physics has been greatly developed starting from the works of Gibbs, Maxwell, and Boltzmann.

First proposed in the late 1960s and since then largely studied, asymmetric simple exclusion models have become paradigmatic models to investigate nonequilibrium stochastic systems, such as biological transport [5], vehicular traffic, growth models and driven diffusive systems (see e.g. [3]).

In particular, the Totally Asymmetric Simple Exclusion Process (TASEP) has been largely studied.

It consists of a one-dimensional lattice of L sites in which particles unidirectionally and stochastically hop from one site to another, where each site can be occupied by at most one particle, subject to hard-core or simple exclusion (meaning two particles cannot occupy the same site)[1].

Different boundary conditions may be chosen, usually periodic boundary conditions or open boundary conditions: in the former case particles live on a ring (a closed one-dimensional lattice) while in the latter case particles live on a segment, they enter at one end of the lattice and exit at the other end.

Seminal works include those of Derrida et al. [4], Schütz and Domany [10] in which analytical and exact results are given for the ordinary case, in which particles jump at unit rates throughout the lattice, with open boundary conditions.

Then many generalizations and variants have been defined and studied taking inspiration from specific real-world vehicular and biological traffic

[1] In chapter 2 a rigorous definition will be given

problems, such as: TASEP with extended particles, TASEP-LK[2], multilane TASEP, multi-species TASEP, TASEP with heterogeneous hopping rates,....

Among the numerous variants, which can easily be found in the literature, a particular case of interest, discussed, for example, by Kolomeisky in [1] or by Greulich and Schadschneider in [8], is TASEP with local inhomogeneities (in the literature also called defects, impurities, slow bonds, ...), which can be treated as a paradigmatic model for investigating transport phenomena in the presence of a bottleneck.

The above mentioned works, and others that can be found in the literature, limit the investigation to the non-equilibrium steady states (NESS)[3].

Following what Botto et al. (see [6], [7]) have done in the case of TASEP-LK, the present Master's Thesis aims at extending the investigation of the relaxation dynamics also to the case of TASEP with local inhomogeneities.

In particular, after discussing the stationary states and the corresponding phase diagram, obtained through the use of the mean-field theory, the long-time relaxation behavior close to stationarity will be discussed and the so-called dynamical transitions, i.e. changes in the relaxation dynamics, will be highlighted.

From a mathematical point of view, the mean-field theory allows us to treat the TASEP as a deterministic dynamical system, neglecting the stochastic nature of the system, to investigate its fixed point solutions and corresponding relaxation behaviour.

In particular, in chapter 2 we will provide definitions and notation that will be used throughout the thesis, in chapter 3 the pure (or ordinary) TASEP will be reviewed, while in chapter 4 the TASEP with local inhomogeneities will be discussed, finally in chapter 5 we will summarize the main results and provide some suggestions for future works.

[2]Langmuir Kinetics, in which particles can attach and detach to and from any site of the lattice.

[3]In this work conveniently called stationary states, steady-states or phases.

Chapter 2

Definitions

2.1 TASEP with Open Boundary Conditions

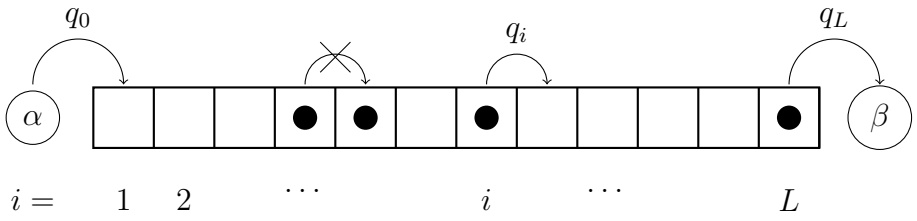

Figure 2.1: Ilustration of TASEP with OBC.

The TASEP is defined on a one-dimensional lattice of L sites, to each site $i \in \{1, 2 \ldots, L\}$ and $\forall t \geq 0$ a binary random variable $n_i(t)$, called the occupation number, is assigned:

$$n_i(t) = \begin{cases} 1, & \text{if site } i \text{ is occupied at time } t \\ 0, & \text{if site } i \text{ is empty at time } t \end{cases} \tag{2.1}$$

Particles stochastically hop from one site to the next with, possibly, position dependent hopping rates $q_i \in [0, 1]$, $i \in \{1, 2, \ldots, L-1\}$, i.e. if $n_i(t) = 1$ and $n_{i+1}(t) = 0$ [1] , then with rate q_i the particle in the lattice site i can hop to the lattice site $i + 1$, whereas the opposite hopping never occurs due to total asymmetry.

Moreover, considering open boundary conditions (OBC), in the first lattice site $i = 1$, particles are injected with an entry/injection rate α, provided

[1] due to the hard-core exclusion.

that $n_1(t) = 0$, while in the last lattice site $i = L$, particles are extracted with an exit/extraction rate β , provided that $n_L(t) = 1$.

Equivalently, mainly for mathematical convenience, one can consider two reservoirs of particles with density $\alpha, (1-\beta) \in [0, 1]$ at the boundaries of the system, which are injected and extracted with additional hopping rates q_0 and q_L, as sometimes will be done in this work.

2.1.1 The Master Equation and Mean-Field theory

Master equation

The system dynamics is governed by a Master Equation (ME) due to the stochastic mechanisms defined above and here summarized:

- injection of particles in the system with rate α,
- hopping of particles inside the system with rates $q_i, i \in \{1, 2, \ldots, L-1\}$,
- extraction of particles from the system with rate β,

all subject to hard-core exclusion.

The states of the system can be denoted by $n = (n_1, \ldots, n_L)$ with $n \in \{0, 1\}^L$, while $P(n, t)$ denotes the probability that the system is in the state n at time t.

Then the ME can be written as:

$$\partial_t P(n,t) = \sum_m [W(m \to n)P(m,t) - W(n \to m)P(n,t)] \tag{2.2}$$

where $W(m \to n)$ is the transition rate of the system moving from state m to state n, in which all the above mechanisms are encoded.

Continuity Equations and Mean-Field approximation

After marginalizing the Master Equation, one obtains in terms of single-node marginals

$$\rho_i(t) := \langle n_i(t) \rangle = \mathbb{P}\{n_i(t) = 1\} \tag{2.3}$$

also called densities, and two-node marginals

$$J_i(t) := q_i \langle n_i(t)(1 - n_{i+1}(t)) \rangle = q_i \mathbb{P}\{n_i(t) = 1, n_{i+1}(t) = 0)\} \tag{2.4}$$

also called currents , where $\langle\ \rangle$ denotes the out-of-equilibrium average, continuity equations of the form:

$$\dot{\rho}_i(t) = J_{i-1}(t) - J_i(t) \tag{2.5}$$

where $J_0(t) = \alpha(1 - \rho_1(t))$ and $J_L(t) = \beta\rho_L(t)$ can be defined to take into account boundary conditions.

Then using mean-field theory, which in this context neglects correlations by approximating joint probabilities with product of single-node marginals:

$$P(n) = \prod_i P(n_i) \tag{2.6}$$

one obtains the mean-field form of the currents:

$$\begin{aligned} J_i(t) &= q_i P(n_i(t) = 1, n_{i+1}(t) = 0) \\ &= q_i P(n_i(t) = 1) P(n_{i+1}(t) = 0) \\ &= q_i \rho_i(t)(1 - \rho_{i+1}(t)), \qquad i = 1, \dots, L-1 \end{aligned} \tag{2.7}$$

Finally, inserting the above into (2.5), a full solution could be in principle obtained by solving the system of equations:

$$\begin{cases} \dot{\rho}_1(t) = \alpha(1 - \rho_1(t)) - q_1\rho_1(t)(1 - \rho_2(t)) \\ \dot{\rho}_i(t) = q_{i-1}\rho_{i-1}(t)(1 - \rho_i(t)) - q_i\rho_i(t)(1 - \rho_{i+1}(t)), \qquad i = 2, \dots, L-1 \\ \dot{\rho}_L(t) = q_{L-1}\rho_{L-1}(t)(1 - \rho_L(t)) - \beta\rho_L(t) \end{cases} \tag{2.8}$$

or by taking into account the boundary conditions through $\alpha =: q_0\rho_0$ and $\beta =: q_L(1-\rho_{L+1})$ (arbitrarily choosing $q_0 = q_L = 1$ in most cases), in a more compact form:

$$\dot{\rho}_i(t) = q_{i-1}\rho_{i-1}(t)(1 - \rho_i(t)) - q_i\rho_i(t)(1 - \rho_{i+1}(t)), \quad i = 1, \dots, L \tag{2.9}$$

where together with the boundary currents $J_0(t)$ and $J_L(t)$ (2.7) can also be written compactly as:

$$J_i(t) = q_i\rho_i(t)(1 - \rho_{i+1}(t)), \qquad i = 0, \dots, L \tag{2.10}$$

In most cases, the above system is analytically intractable and can only be solved numerically.

2.1.2 Stationary states and Relaxation to stationarity

Sometimes one is not interested in the full dynamics but only what happens at stationarity, i.e. when the system state does not change anymore, and in the relaxation behaviour, which does not necessarily need the full solution.

Stationary states

To obtain stationary states, one has to impose the condition that the observables do not change in time: $\rho_i(t) \to \rho_i$, $J_i(t) \to J_i$. In particular, this implies that the currents $J_i(t)$ are both time-invariant and position-independent:

$$J_{i-1}(t) = J_i(t) = J, \qquad \forall i \in \{1, 2, \ldots, L\} \tag{2.11}$$

which implies that the densities must satisfy:

$$q_{i-1}\rho_{i-1}(1-\rho_i) = q_i\rho_i(1-\rho_{i+1}) \quad \forall i \in \{1, 2, \ldots, L\} \tag{2.12}$$

which can be written as:

$$\rho_i = \left(1 + \frac{q_i(1-\rho_{i+1})}{q_{i-1}\rho_{i-1}}\right)^{-1} \quad \forall i = 1, \ldots, L \tag{2.13}$$

with boundary conditions

$$\begin{cases} \rho_0 = \alpha \\ \rho_{L+1} = 1 - \beta \end{cases} \tag{2.14}$$

using $q_0 = q_L = 1$.

The above form is readily suitable for a fixed point procedure that generates a sequence of density profiles that converges [2] to the solution (a proof for a particular case can be found in [6]).

Relaxation matrix

Following the same procedure as in [2, 6, 7], we can linearize the continuity equations (2.9) around the steady-state fixed point densities ρ_i:

$$\dot{\rho}_i(t) = -\sum_{j=1}^{L} M_{i,j}\big(\rho_j(t) - \rho_j\big), \qquad i = 1, \ldots, L \tag{2.15}$$

where $M \in \mathbb{R}^{L\times L}$, defined as

$$M_{i,j} := -\frac{\partial \dot{\rho}_i(t)}{\partial \rho_j}\bigg|_{t\to+\infty}, \qquad i, j \in \{1, \ldots, L\} \tag{2.16}$$

is the so-called *relaxation matrix* associated to the TASEP.

[2] In practice, one chooses a tolerance condition such as $max\{|\rho_i^{n+1} - \rho_i^n|, i = 1, \ldots, L\} < \epsilon$ to be satisfied and stops the process obtaining a reasonable approximate solution (n represents the iteration step)

It takes non-vanishing values:

$$\begin{cases} M_{i,i} = q_{i-1}\rho_{i-1} + q_i(1-\rho_{i+1}), & i = 1,\dots,L, \\ M_{i,i-1} = -q_{i-1}(1-\rho_i), & i = 2,\dots,L, \\ M_{i,i+1} = -q_i\rho_i, & i = 1,\dots,L-1 \end{cases} \tag{2.17}$$

resulting in a tridiagonal matrix.

The spectrum of this matrix characterizes relaxation to stationarity and in particular its lowest eigenvalue corresponds to the slowest relaxation rate, i.e. the inverse of the longest relaxation time.

Then, one can write the associated eigenvalue problem:

$$M_{i,i}v_i + M_{i,i-1}v_{i-1} + M_{i,i+1}v_{i+1} = \lambda v_i \qquad i = 1,\dots,L \tag{2.18}$$

where λ is the eigenvalue and the v_i are the eigenvector components with $v_0 = v_{L+1} = 0$.

Following [6], a similarity transformation of M can be performed, using:

$$u_n \equiv v_n \prod_{j=0}^{n-1} \sqrt{\frac{\rho_j}{1-\rho_{j+1}}} \qquad n = 0,\dots,L+1 \tag{2.19}$$

with $u_0 = u_{L+1} = 0$, to obtain a symmetrized eigenvalue problem:

$$M_{i,i}u_i - \sqrt{q_{i-1}J}u_{i-1} - \sqrt{q_iJ}u_{i+1} = \lambda u_i \qquad i = 1,\dots,L \tag{2.20}$$

where the explicit expression of M and the fact that in stationary conditions $J = q_i\rho_i(1-\rho_{i+1}), \forall i = 0,\dots,L$ were used.

In general, one has to resort to numerical algorithms.

For example, the results that will be presented in this work are obtained through the use of functions (such as eigvals) of the LinearAlgebra package of Julia programming language, which are based on LAPACK (Linear Algebra Package), a standard software library for numerical linear algebra employed by scientific computing software such as MATLAB or R.

2.2 Cases of interest

We will now define two particular classes of TASEP with OBC that will be used or analyzed in this work: uniform or homogeneous TASEP and TASEP with local inhomogeneities.

2.2.1 Homogeneous TASEP

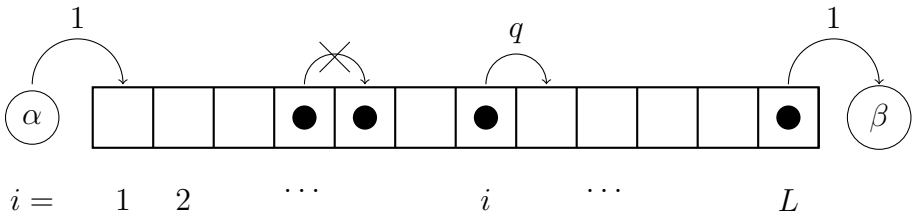

Figure 2.2: Illustration of Homogeneous TASEP of parameter q with OBC

The homogeneous or uniform TASEP is characterized by hopping rates q_i of the form:

$$q_i = \begin{cases} 1, & i = 0, L \\ q, & i = 1, \dots, L-1 \end{cases} \tag{2.21}$$

where $q > 0$ is the same for all sites (apart from q_0 and q_L).

Continuity equations (2.8) take the simple form:

$$\begin{cases} \dot{\rho}_1(t) = \alpha(1-\rho_1(t)) - q\rho_1(t)(1-\rho_2(t)) \\ \dot{\rho}_i(t) = q\rho_{i-1}(t)(1-\rho_i(t)) - q\rho_i(t)(1-\rho_{i+1}(t)), \qquad i = 2, \dots, L-1 \\ \dot{\rho}_L(t) = q\rho_{L-1}(t)(1-\rho_L(t)) - \beta\rho_L(t) \end{cases} \tag{2.22}$$

with currents being:

$$\begin{cases} J_0(t) = \alpha(1-\rho_1(t)) \\ \qquad\qquad\qquad\qquad J_i(t) = q\rho_i(t)(1-\rho_{i+1}(t)), \\ \qquad i = 1, \dots, L-1 \\ J_L(t) = \beta\rho_L(t) \end{cases} \tag{2.23}$$

In the literature, homogeneous TASEP is rarely defined as above but directly as the special case $q = 1$ (maintaining $q_0 = q_L = 1$).

This is due to the fact that a TASEP of injection rate α, extraction rate β and hopping rates q with current J is equivalent to a TASEP of injection

rate $\frac{\alpha}{q}$, extraction rate $\frac{\beta}{q}$ and unitary hopping rates with current J/q, i.e. the TASEP is invariant under the transformation[3]:

$$(\alpha, \beta, q, J) \to (\frac{\alpha}{q}, \frac{\beta}{q}, 1, \frac{J}{q}) \tag{2.24}$$

Additionally, under the hypothesis $q_0 = q_L$, the (pure) TASEP is symmetric under the transformation $\alpha \leftrightarrow \beta$, $1 - n_i \leftrightarrow n_{L+1-i}$ (called particle–hole symmetry), sometimes this property will be invoked.

2.2.2 TASEP with local inhomogeneities

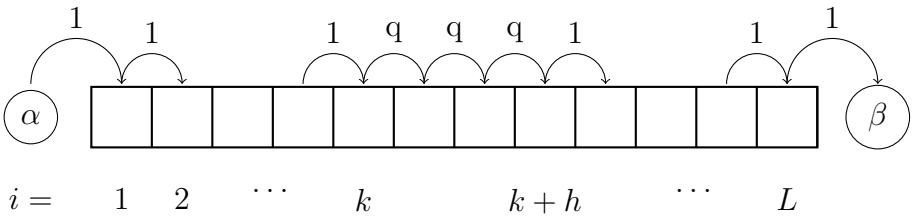

Figure 2.3: TASEP scheme with OBC and local inhomogeneities

Let us proceed to define the main model that will be analyzed in the present work.

It is a TASEP with OBC with a particular choice of hopping rates:

$$q_i = \begin{cases} q, & \text{if} \quad i \in \{k, \dots, k+h-1\} \\ 1, & \text{otherwise} \end{cases} \tag{2.25}$$

as seen in Figure 2.3.

Continuity equations (2.9) take the particular form:

$$\begin{cases} \dot{\rho}_i(t) = \rho_{i-1}(t)(1-\rho_i(t)) - \rho_i(t)(1-\rho_{i+1}(t)), & 1 \le i < k \\ \dot{\rho}_k(t) = \rho_{k-1}(t)(1-\rho_k(t)) - q\rho_k(t)(1-\rho_{k+1}(t)), & \\ \dot{\rho}_i(t) = q\rho_{i-1}(t)(1-\rho_i(t)) - q\rho_i(t)(1-\rho_{i+1}(t)), & k < i < k+h \\ \dot{\rho}_{k+h}(t) = q\rho_{k+h-1}(t)(1-\rho_{k+h}(t)) - \rho_{k+h}(t)(1-\rho_{k+h+1}(t)), & \\ \dot{\rho}_i(t) = \rho_{i-1}(t)(1-\rho_i(t)) - \rho_i(t)(1-\rho_{i+1}(t)), & k+h < i \le L \end{cases} \tag{2.26}$$

[3]One should also consider the transformation $dt \to qdt$, however since we are not interested in the full dynamics we will treat it as a negligible detail.

while currents (2.10), using $q_0 = q_L = 1$,take the form:

$$\begin{cases} J_i(t) = \rho_i(t)(1 - \rho_{i+1}(t)), & 0 \leq i < k, k + h \leq i \leq L \\ J_i(t) = q\rho_i(t)(1 - \rho_{i+1}(t)), & k \leq i \leq k + h - 1 \end{cases} \tag{2.27}$$

The hopping rate q [4], the length h (in units of lattice steps) and the position of the site k are the main parameters of the model, in addition to the usual boundary rates α, β and the length of the lattice L.

In the following chapters we will discuss in more detail the above defined particular models: starting from a review of the homogeneous TASEP, we will move onto the special cases of local inhomogeneities with $h = 1$ and $h = 2$ (sometimes called one-step and two step inhomogeneity).

[4]In this work, we consider only $q < 1$ to model bottleneck effects, since q = 1 would result in the homogeneous case.

Chapter 3

Homogeneous TASEP: main results

In this chapter, we will present the main (mean-field) results for the uniform TASEP and, in particular, due to the invariance of TASEP with respect to (2.24), the case $q = 1$, from now on also called the ordinary or pure case.

The results presented here can easily be found in the literature, see e.g. [10] or [3] for the phase diagram and [2, 6, 7], for the relaxation to stationarity.

When possible, results of the general case $q > 0$ will be made explicit, mainly exploiting the above recalled invariance.

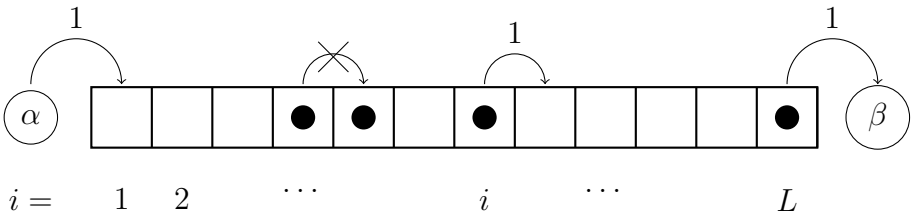

Figure 3.1: Illustration of ordinary TASEP.

In ordinary TASEP, the only parameters to be considered are the injection and extraction rates α, β and the number of lattice sites L, assumed to be in the thermodynamic limit ($L \to \infty$).

The mean-field continuity equations (2.9) reduce to:

$$\dot{\rho}_i(t) = \rho_{i-1}(t)(1 - \rho_i(t)) - \rho_i(t)(1 - \rho_{i+1}(t)), \quad i = 1, \ldots, L \tag{3.1}$$

with boundary conditions $\rho_0 = \alpha$ and $\rho_{L+1} = 1 - \beta$.

3.1 Stationary states and phase diagram

Imposing stationarity, the above equations then reduce to equations (2.13) that allow one to obtain fixed-point solutions, in the following summarized:

- for $\alpha < \frac{1}{2}$ and $\alpha < \beta$ there exists a **low-density (LD)** phase characterized by bulk density $\rho_{bulk} = \alpha$ and a right (dependent on β) boundary layer, the stationary current is $J = \alpha(1 - \alpha)$;

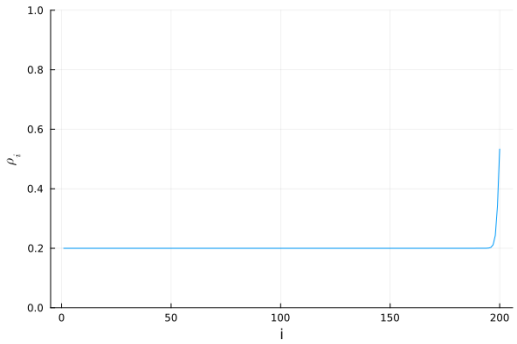

Figure 3.2: Example of mean-field density profile in the LD phase ($L = 200$, $\alpha = 0.2$, $\beta = 0.3$).

- for $\beta < \frac{1}{2}$ and $\beta < \alpha$ there exists a **high-density (HD)** phase characterized by bulk density $\rho_{bulk} = 1 - \beta$ and a left (dependent on α) boundary layer, the stationary current is $J = \beta(1 - \beta)$;

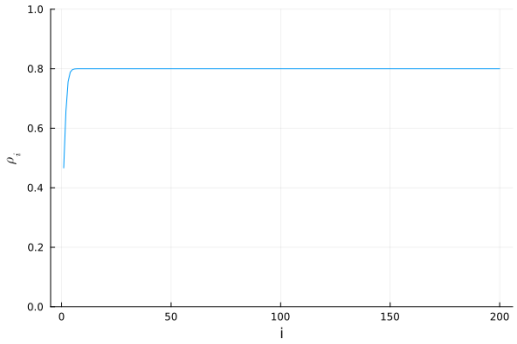

Figure 3.3: Example of mean-field density profile in the HD phase ($L = 200$, $\alpha = 0.3$, $\beta = 0.2$).

- for $\alpha > \frac{1}{2}$ and $\beta > \frac{1}{2}$ there exists a **maximal current (MC)** phase characterized by the maximal stationary current $J = 1/4$ and a profile density approaching the "bulk"[1] density $\rho_{bulk} = \frac{1}{2}$.

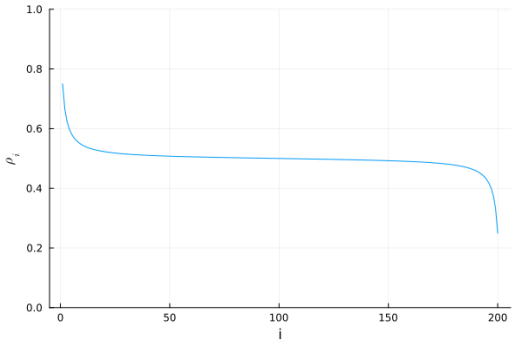

Figure 3.4: Example of mean-field density profile in the MC phase ($L = 200$, $\alpha = 1$, $\beta = 1$).

The above can also be schematized in a phase diagram (α-β plane):

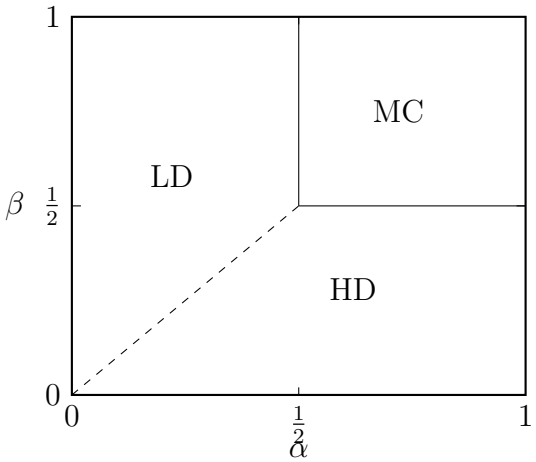

Figure 3.5: Mean-field phase diagram. Solid lines denote continuous phase transitions, dashed line denotes discontinuous phase transition.

The lines depicted in the figure above represent the phase transition lines: the LD-HD transition ($\alpha = \beta < 1/2$) is discontinuous while the LD-MC ($\beta > \alpha = 1/2$) and HD-MC ($\alpha > \beta = 1/2$) transition lines are continuous. Despite

[1] In the MC phase the approach to the bulk density is a power law decay, whereas in the other two phases is an exponential decay.

the mean-field approximation, the above diagram is exact with respect to the position of the transition lines and values of the bulk densities and currents.

Generalizing to the case $q > 0$, we have that the transition point $\alpha = \beta = 1/2$ is shifted to $\alpha = \beta = q/2$ and the maximal current is $J = q/4$ instead of $J = 1/4$.

3.2 Relaxation matrix and dynamical transitions

The relaxation matrix (2.17) takes non-vanishing values:

$$\begin{cases} M_{i,i} = \rho_{i-1} + (1 - \rho_{i+1}), & i = 1, \dots, L, \\ M_{i,i-1} = -(1 - \rho_i), & i = 2, \dots, L, \\ M_{i,i+1} = -\rho_i, & i = 1, \dots, L-1 \end{cases} \tag{3.2}$$

which reduce the symmetrized eigenvalue problem (2.20) into:

$$M_{i,i}u_i - \sqrt{J}u_{i-1} - \sqrt{J}u_{i+1} = \lambda u_i \qquad i = 1, \dots, L \tag{3.3}$$

In general, as already said in chapter 2, one has to resort to a numerical algorithm to compute eigenvalues and eigenvectors. However, if we consider for a moment the particular case of a flat density profile, which is actually obtained for $\alpha + \beta = 1$, the above problem reduces to:

$$u_i - \sqrt{J}u_{i-1} - \sqrt{J}u_{i+1} = \lambda u_i \qquad i = 1, \dots, L \tag{3.4}$$

(with $u_0 = u_{L+1} = 0$), which is analytically solvable because M takes the form of a Toeplitz (or diagonal-constant) matrix.

In fact, calling $x_\pm(\lambda)$ the (complex) solutions of the characteristic equation

$$x^2 - \left(\frac{1-\lambda}{\sqrt{J}}\right) x + 1 = 0 \tag{3.5}$$

one can prove (see Appendix) that the eigenvalue problem above is solved by

$$u_n = u_1 \frac{x_+^n - x_-^n}{x_+ - x_-}, \qquad n = 1, 2, \dots, L \tag{3.6}$$

with eigenvalues

$$\lambda_j = 1 - 2\sqrt{J}\cos\frac{\pi j}{L+1}, \qquad j = 1, \dots, L \tag{3.7}$$

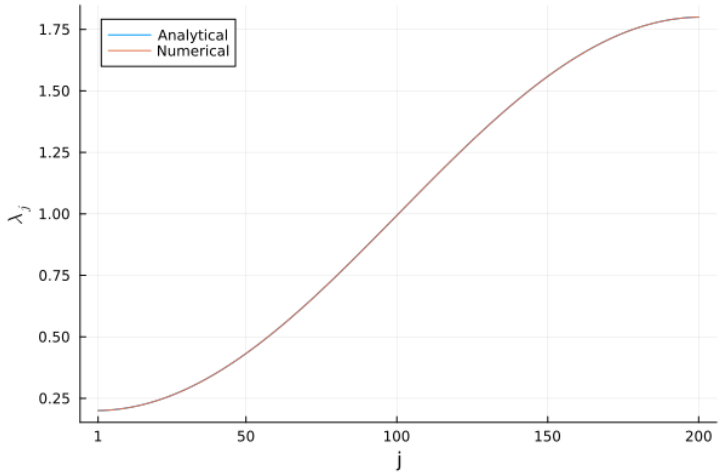

Figure 3.6: Spectrum in the case of a flat density profile ($\alpha + \beta = 1$) for $L = 200$ and $J = 0.16$ (e.g. $\alpha = 0.8, \beta = 0.2$), the largest (absolute) difference is slightly less than $6 \cdot 10^{-9}$.

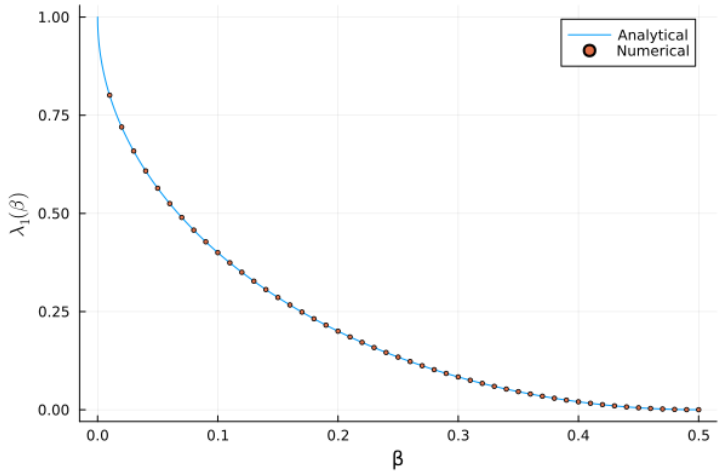

Figure 3.7: Numerical and analytical results of the lowest relaxation rate as a function of β (for $\alpha + \beta = 1$) for $L = 200$, the largest (absolute) difference is less than $5 \cdot 10^{-6}$. Values for $\beta \geq 1/2$ are not shown, since in this range we have $J = 1/4$ and $\lambda_1 \to 0$ as $O(L^{-2})$ for $L \to \infty$

In the $L \to \infty$ limit, the smallest eigenvalue (i.e. the slowest relaxation rate) tends to $\lambda_1 = 1 - 2\sqrt{J}$.

As a check, let us compare the above analytical results with the numerical eigenvalues. For the example shown in Figure 3.6 there is very good agreement between the numerically evaluated spectrum and the analytical one (3.7). In particular, if we consider only the lowest relaxation rate (as a function of β [2], with $\alpha + \beta = 1$), there is still good agreement as shown in Figure 3.7.

Let us move on from the special case of a flat profile and to fix ideas consider lines of constant β in the HD phase.

One finds that the above picture remains qualitatively[3] correct for values of α larger than a threshold value $\alpha_c(\beta)$ (in which λ_1 is independent of α[4]), while for values of α in the interval $(\beta, \alpha_c(\beta))$ the picture drastically changes with the lowest relaxation rate (now dependent on both α and β) being smaller than the limit value $1 - 2\sqrt{J}$.

For example, in Figure 3.8 the value of the lowest relaxation rate is plotted as a function of α for $\beta = 0.2$ where, as said above, a threshold can be seen. Moreover, one can notice that λ_1 goes to 0 for $\alpha = \beta$ where the discontinuous (static) transition is located.

The critical values $\alpha_c(\beta)$ in the HD phase and $\beta_c(\alpha)$ in the LD phase (can be found by invoking the symmetry property stated at the end of subsection 2.2.1) become critical lines in the phase diagram, which denote the presence of *dynamical transitions* that do not correspond to any (static) phase transition, in contrast to the LD/HD and the LD/HD-MC transition lines, in which the lowest relaxation rate vanishes, which we should also consider as dynamical transition lines (see Figure 3.9 for the complete phase diagram).

For completeness (even though they will not be used in this work) we report the exact [9] critical values:

$$\alpha_c(\beta) = \left[1 + \left(\frac{\beta}{1-\beta})\right)\right]^{-1}, \qquad \beta \in [0, 1/2] \tag{3.8}$$

$$\beta_c(\alpha) = \left[1 + \left(\frac{\alpha}{1-\alpha})\right)\right]^{-1}, \qquad \alpha \in [0, 1/2] \tag{3.9}$$

[2] Only values of $\beta \in [0, \frac{1}{2}]$ are shown since $J = \beta(1-\beta) = \alpha(1-\alpha)$ if $\alpha + \beta = 1$.

[3] and quantitatively up to finite-size corrections.

[4] This also means that lines of constant α (above the critical values $\alpha_c(\beta)$) show the same behavior as the line $\alpha + \beta = 1$.

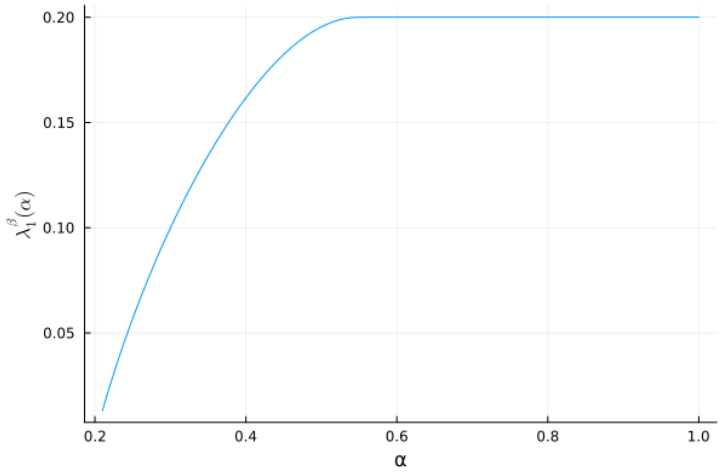

Figure 3.8: Lowest relaxation rate as a function of α for fixed $\beta = 0.2$ in the HD phase ($L = 200$).

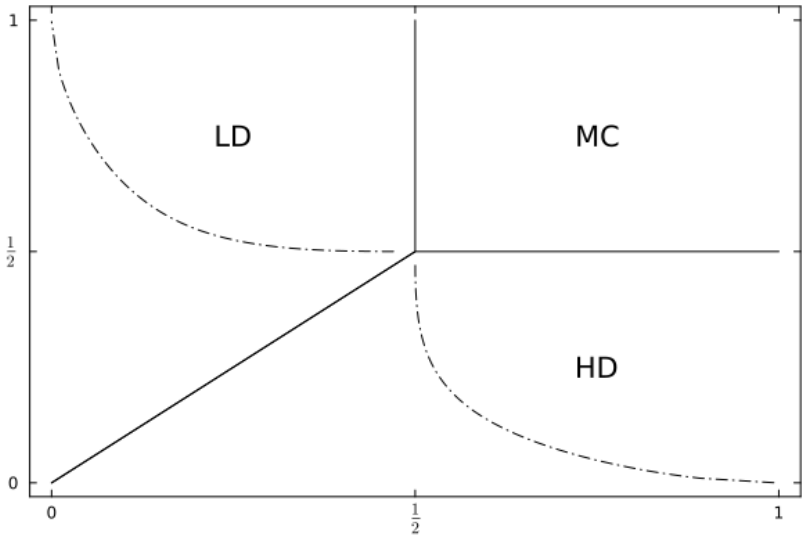

Figure 3.9: Pure TASEP (complete) phase diagram. Static transitions are depicted by solid lines, dynamical transitions are depicted by thin dash-dotted lines.

Chapter 4

TASEP with local inhomogeneities

Let us proceed to present and discuss the case of TASEP with local inhomogeneities.

As said in chapter 2, the parameters to consider are not only the rates α, β and the length of the lattice L (still assumed to be in the thermodynamic limit) but also the length of the inhomogeneities h, with corresponding initial site k, and the hopping rate q.

In particular, in this discussion, h will be treated as a defining parameter of the model, which means that two TASEP with different h will be treated as different models, while k is only subject to the constraint that it must be far from boundaries, i.e. $k \approx L/2$.

As we shall see, the overall picture of stationary states and relaxation behaviour is richer (and different) than the ordinary TASEP one.

It is important to remind the reader that we employ the mean-field theory to investigate in the simplest way the relaxation behaviour of the TASEP.

However, by applying more sophisticated methods and techniques, such as those used by Kolomeisky in [1] or by Greulich and Schadschneider in [8], more accurate results regarding stationary states have been obtained, compared to Monte Carlo methods which simulate the exact dynamics of the system.

4.1 One-step inhomogeneity ($h = 1$)

Let us start with the case where the region of inhomogeneities is of length 1 (in units of lattice steps).

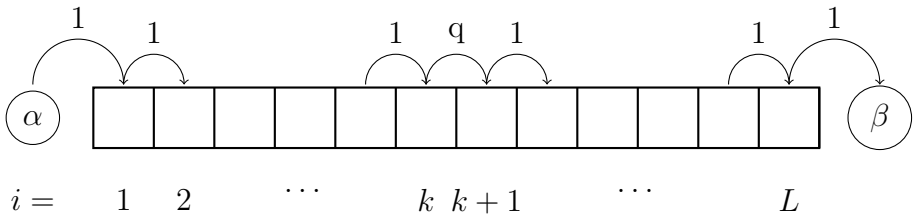

Figure 4.1: Illustration of TASEP with local inhomogeneities of length $h = 1$ with hopping rate q, placed between sites k and $k + 1$.

In the case of $h = 1$ the continuity equations (2.26) reduce to:

$$\begin{cases} \dot{\rho}_i(t) = \rho_{i-1}(t)(1 - \rho_i(t)) - \rho_i(t)(1 - \rho_{i+1}(t)), & i \neq k, k+1 \\ \dot{\rho}_k(t) = \rho_{k-1}(t)(1 - \rho_k(t)) - q\rho_k(t)(1 - \rho_{k+1}(t)), & \\ \dot{\rho}_{k+1}(t) = q\rho_k(t)(1 - \rho_{k+1}(t)) - \rho_{k+1}(t)(1 - \rho_{k+2}(t)), & \end{cases} \tag{4.1}$$

with currents (2.27) being

$$\begin{cases} J_i(t) = \rho_i(t)(1 - \rho_{i+1}(t)), & i \neq k \\ J_k(t) = q\rho_k(t)(1 - \rho_{k+1}(t)). & \end{cases} \tag{4.2}$$

4.1.1 Stationary states and Phase diagram

Once stationarity is imposed, one can solve the resulting sytem of equations

$$\begin{cases} \rho_{i-1}(1 - \rho_i) = \rho_i(1 - \rho_{i+1}), & i \neq k, k+1 \\ \rho_{k-1}(1 - \rho_k) = q\rho_k(1 - \rho_{k+1}), & (i = k) \\ q\rho_k(1 - \rho_{k+1}) = \rho_{k+1}(1 - \rho_{k+2}), & (i = k+1) \\ \rho_0 = \alpha, \quad \rho_{L+1} = 1 - \beta, & \end{cases} \tag{4.3}$$

and obtain the following:

- for $\alpha < q/(q + 1)$ and $\alpha < \beta$ there exists a **low-density (LD)** phase (an example can be seen in Figure 4.2) characterized by a bulk density $\rho_{bulk} = \alpha$ and stationary current $J = \alpha(1-\alpha)$ (as in the ordinary case) with two boundary layers, a right boundary layer (dependent on β) as in pure TASEP and an additional layer on the left side of k, dependent on α and q, with $\rho_k = \alpha/q$ and $\rho_{k+1} = \alpha$;

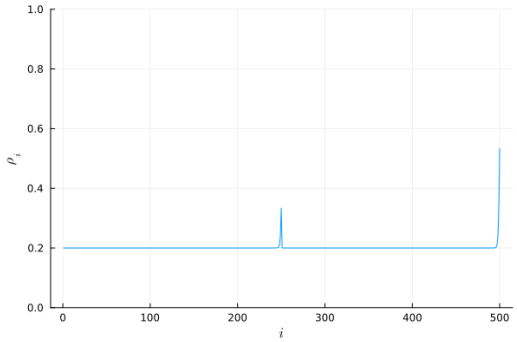

Figure 4.2: Example of mean-field density profile in the LD phase for $h = 1$ ($L = 500$, $\alpha = 0.2$, $\beta = 0.3$, $q = 0.6$).

- for $\beta < q/(q+1)$ and $\beta < \alpha$ there exists a **high-density (HD)** phase (an example can be seen in Figure 4.3) characterized by a bulk density $\rho_{bulk} = 1 - \beta$ and stationary current $J = \beta(1 - \beta)$ (as in the ordinary case) with two boundary layers, a left boundary layer (dependent on α) as in pure TASEP and an additional layer on the right side of k, dependent on β and q, with $\rho_k = 1 - \beta$ and $\rho_{k+1} = 1 - \beta/q$;

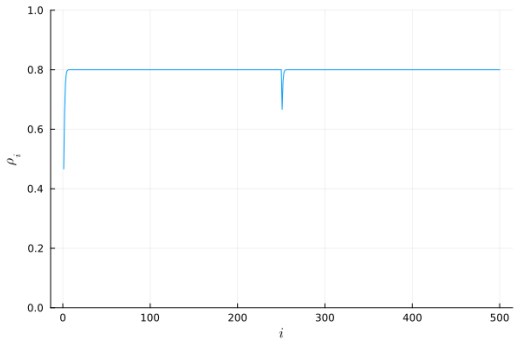

Figure 4.3: Example of mean-field density profile in the HD phase for $h = 1$ ($L = 500$, $\alpha = 0.3$, $\beta = 0.2$, $q = 0.6$).

- for $\alpha \geq q/(q+1)$ and $\beta \geq q/(q+1)$ there exists a **maximal current (MC))** phase or **phase separation (PS)** regime (an example can be seen in Figure 4.4) characterized by two bulk densities $\rho_{bulk,left} = 1/(q+1)$, $\rho_{bulk,right} = q/(q+1)$ (with $\rho_k = \rho_{bulk,left}$, $\rho_{k+1} = \rho_{bulk,right}$) and maximal current $J = q/(q+1)^2$ with two boundary layers, a left boundary layer dependent on α and a right boundary layer dependent on β;

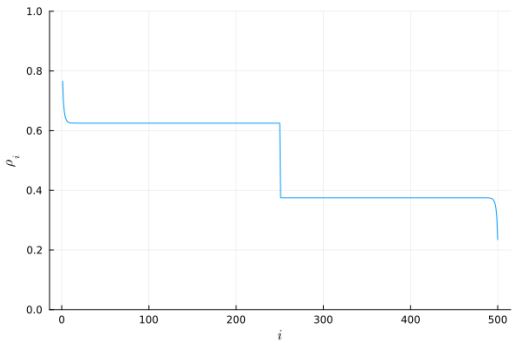

Figure 4.4: Example of mean-field density profile in the PS regime for $h = 1$ ($L = 500$, $\alpha = 1$, $\beta = 1$, $q = 0.6$).

Reporting the above results in an α-β plane, we obtain the (static) phase diagram sketched in Figure 4.5.

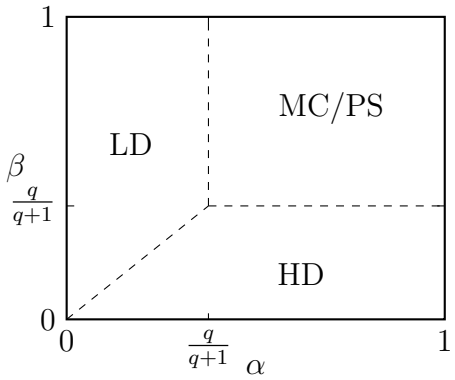

Figure 4.5: Mean-field phase diagram for $h = 1$. Dashed line denote discontinuous phase transition.

As one can see in the Figure 4.5, the depicted lines represent phase transitions: mean-field theory predicts that all phase transitions are discontinuous (argued also by [8]). Moreover, in contrast to the pure case, the transition point $\alpha = \beta = q/(q + 1)$ now depends on q.

It is worth repeating that, for the case of local inhomogeneities, the maximal current state is a phase separation regime: particles have a higher bulk density on the left of the inhomogeneity site and a lower bulk density on the right of inhomogeneity lattice site.

At least on a qualitative level, the system state tells us that the local inhomogeneity is effectively behaving as a bottleneck. Using traffic analogy:

traffic is slower and denser before the bottleneck, faster and less dense after it.

Instead, in the other two phases, the system seems to be only locally perturbed with respect to the ordinary TASEP case, at least regarding steady-states. In fact, if one were to superimpose, for example, Figure 3.3 with Figure 4.3 the only (visual) difference would be the "spike" around the inhomogeneity.

However, as we shall see, the presence of the inhomogeneity radically changes, with respect to ordinary TASEP, the relaxation behaviour.

4.1.2 Relaxation matrix and dynamical transitions

The symmetrized eigenvalue problem 2.20 takes the form :

$$\begin{cases} M_{i,i}u_i - \sqrt{J}u_{i-1} - \sqrt{J}u_{i+1} = \lambda u_i, & i \neq k, k+1 \\ M_{k,k}u_k - \sqrt{J}u_{k-1} - \sqrt{qJ}u_{k+1} = \lambda u_k, & (i = k) \\ M_{k+1,k+1}u_{k+1} - \sqrt{qJ}u_k - \sqrt{J}u_{k+2} = \lambda u_{k+1}, & (i = k+1) \end{cases} \tag{4.4}$$

with, as usual, $u_0 = u_{L+1} = 0$.

To investigate the relaxation behaviour, we first consider q to be fixed and study λ_1 (and sometimes λ_2) as a function of α and β.

In the following numerical results will be presented.

HD phase: lines of constant β

Keeping in mind Figure 3.8, we consider λ_1 (and λ_2 for further discussion) as function of α, for $\alpha > \beta$, with constant β.

As one can see in Figure 4.7, the lowest eigenvalue (depicted in blue) shows a threshold behaviour for some $\alpha = \alpha_c(\beta)$ [1]: for $\alpha > \alpha_c(\beta)$ the lowest rate remains constant and independent of α while for $\alpha < \alpha_c(\beta)$ the rate is smaller than the plateau value and, in particular, it vanishes for $\alpha = \beta$, similarly to the ordinary case.

A clearer picture can be obtained by directly comparing or superimposing the two above mentioned Figures 3.8 and 4.7: the threshold point can be interpreted as the intersection between the lowest rate of a pure TASEP (of boundary rates α and β) and a constant line, whose value depends on β and q due to the presence of the inhomogeneity. However, numerical evidence suggests that for some interval of values of q the above picture can be

[1] different from the pure TASEP one.

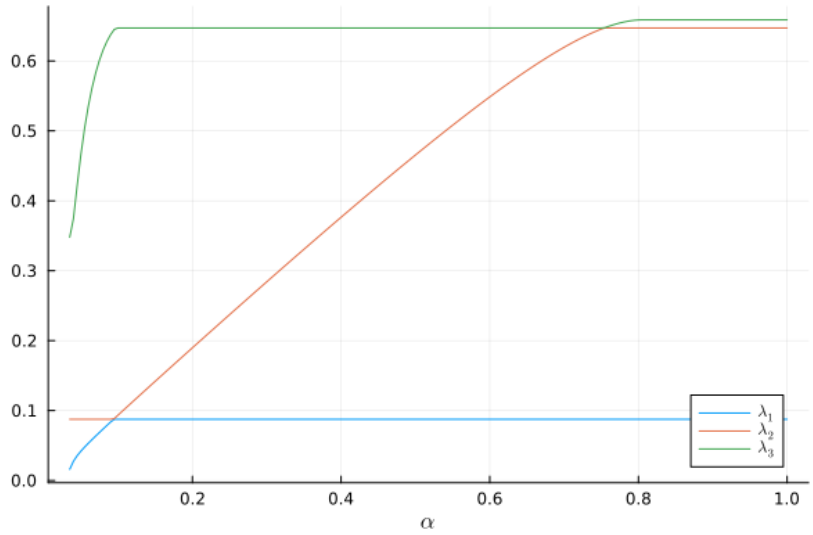

Figure 4.6: The three lowest eigenvalues as function of α for $q = 0.1$ ($L = 1000, \beta = 0.03$).

seen only if one takes in consideration also λ_3, in which two constant values intersect the pure TASEP rate, as seen in Figure 4.6.

The above mentioned threshold is easily interpreted as a *dynamical transition*, similar to the pure TASEP case. In Figure 4.8 the dynamical transition lines (numerically evaluated) are shown, separating a region in which the lowest rate is a function of both boundary rates but independent of q, $\lambda_1 \equiv \lambda_1(\alpha, \beta)$, from a region in which it is independent of α but dependent on q and β, $\lambda_1 \equiv \lambda_1^q(\beta)$.

In summary ,the relaxation behaviour shows an overall similarity to the pure case: there is a region of the phase diagram in which the lowest relaxation rate is independent of α; moreover, the lowest rate decreases with increasing β and goes to zero for $\beta = q/(q+1)$, similar to how ordinary TASEP lowest rate behaves. However, one can observe that the transition described above is of a different kind with respect to that of the pure TASEP; they differ in differentiability (in particular with respect to α at constant β): the ordinary case transition is singular in the second derivative, while in the $h = 1$ case, the transition is singular in the first derivative.

In the above sense, the transition is more similar, at least in some particular cases, to that of the unbalanced TASEP with Langmuir kinetics investigated by Botto et.al in [7] (see Figure 4 of [7]): the transition appears as an avoided crossing between the eigenvalues (see e.g. Figure 4.7).

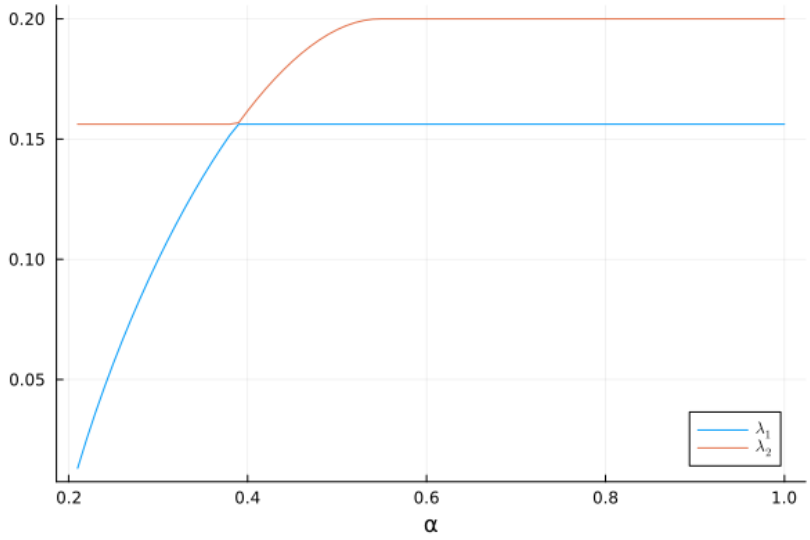

Figure 4.7: The first two lowest eigenvalues as function of α and constant $\beta = 0.2$ ($L = 1000$, $q = 0.6$, $k = 500$). The blue line depicts the lowest rate λ_1, the orange line depicts the second lowest rate λ_2.

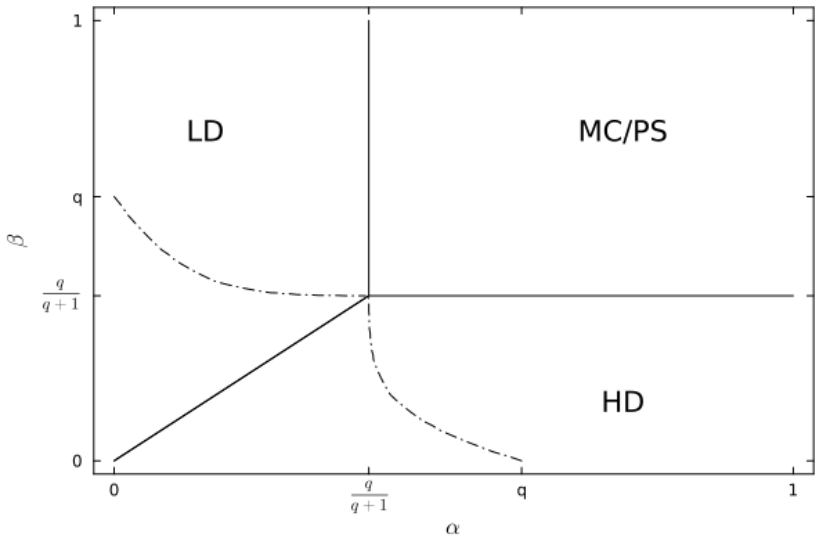

Figure 4.8: Mean-field phase diagram with HD phase dynamical transition lines. Solid lines depict static phase transitions, thin dash-dotted lines depict mean-field (numerical) dynamical transitions.

It is important to note that the relaxation behavior in the LD phase region can easily be obtained by symmetry, recalling property (2.24) (which is also valid [2] in the case we are considering).

[2] as stated in [8], the symmetry transformation would also change the position of the inhomogeneity, however if it is far from the boundaries then the transformation would leave it far from the boundaries.

MC/PS phase: lines of constant α

Let us now shift the focus on the MC/PS phase, where the relaxation behaviour differs from the ordinary TASEP.

In particular, we start by considering λ_1 (and λ_2 if necessary) on lines of constant α.

For example, in Figure 4.9 the smallest eigenvalue λ_1 is plotted as a function of $\beta \geq q/(q+1)$ for $\alpha = 1$. In contrast to the pure case, the lowest rate is zero only for $\beta = q/(q+1)$ and non-zero for any $\beta > q/(q+1)$; moreover λ_1 shows a *dynamical transition* in which, for β greater than a threshold value β^*, it reaches a plateau dependent on q through the maximal current $J = q/(q+1)^2$, formally $\lambda_1 \equiv \lambda_1^q$. Moreover, the threshold value β^* is found to depend on q and the threshold behaviour is found for any $\alpha \geq \beta^*$ (and symmetrically for any $\beta \geq \alpha^* = \beta^*$ when considering constant β instead).

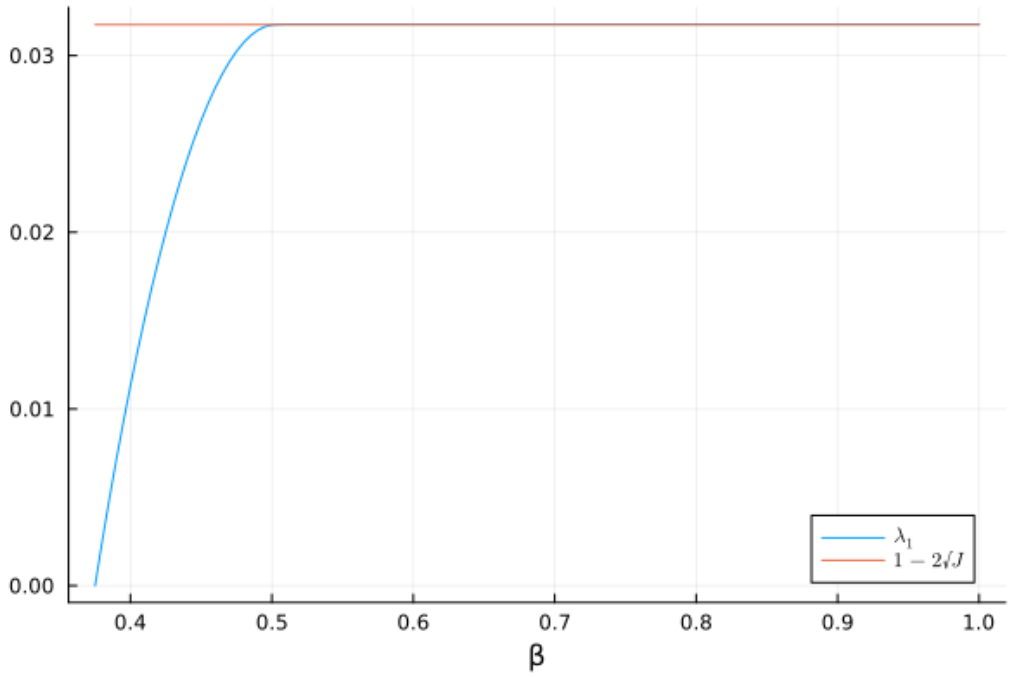

Figure 4.9: Lowest rate λ_1 as a function of β for $\alpha = 1$ ($L = 1000, q = 0.6, k = 500$), depicted in blue, together with the constant value $1 - 2\sqrt{J}$, for $J = q/(q+1)^2$, depicted in orange. Numerical evidence suggests that the difference between the constant value and the rate λ_1 at high β is due to numerical errors and finite-size effects.

If, instead, we consider a constant $\alpha < \beta^*$ a similar, yet different, picture is obtained, as one can see in the following figure: the smallest eigenvalue shows a threshold behaviour (with threshold equal to α) in which the plateau value is lower than the limit value $1 - 2\sqrt{J}$.

Moreover, the overall picture reminds us of the dynamical transition in the HD phase where the lowest rate is independent of α (see Figure 4.7).

In fact, the complete behaviour of λ_1 in the PS region can be summarized as follows:

- for $\alpha > \beta$ and $\beta \in (q/(q+1), \beta^*)$ the rate is independent of α, and we can write $\lambda_1 \equiv \lambda_1^q(\beta)$,
- for $\beta > \alpha$ and $\alpha \in (q/(q+1), \alpha^*)$ the rate is independent of β, and we can write $\lambda_1 \equiv \lambda_1^q(\alpha)$,
- for $\alpha \geq \alpha*, \beta \geq \beta^*$ the rate is independent of both boundary rates and only dependent on q through J ($\lambda_1 \equiv \lambda_1^q$).

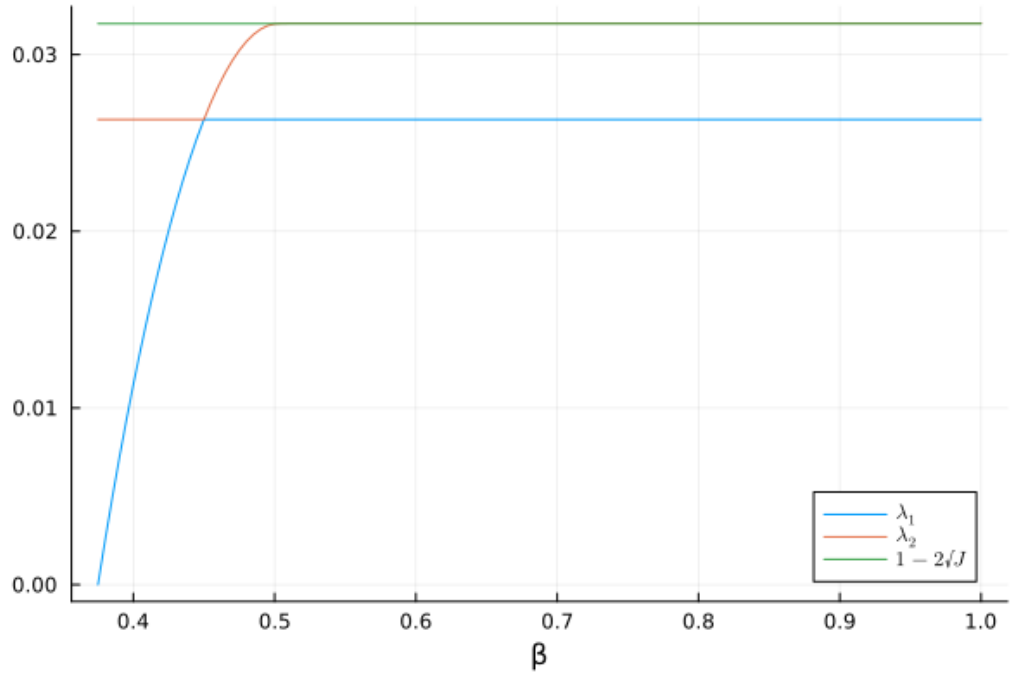

Figure 4.10: Lowest rate λ_1 as a function of β for $\alpha = 0.45$ ($L = 1000, q = 0.6, k = 500$), depicted in blue, together with the second lowest rate λ_2, depicted in orange and the constant value $1 - 2\sqrt{J}$, for $J = q/(q+1)^2$, depicted in green.

The complete lowest relaxation rate "landscape" can also be visualized through a phase diagram, sketched in Figure 4.11, where the dependence of λ_1 on the parameters α, β and q is made explicit.

In particular, one has that in the region below the HD phase dynamical transition the lowest rate is independent of q but dependent on α and β, while above the MC/PS phase dynamical transition the lowest rate is independent of α and β but dependent on q [3] .

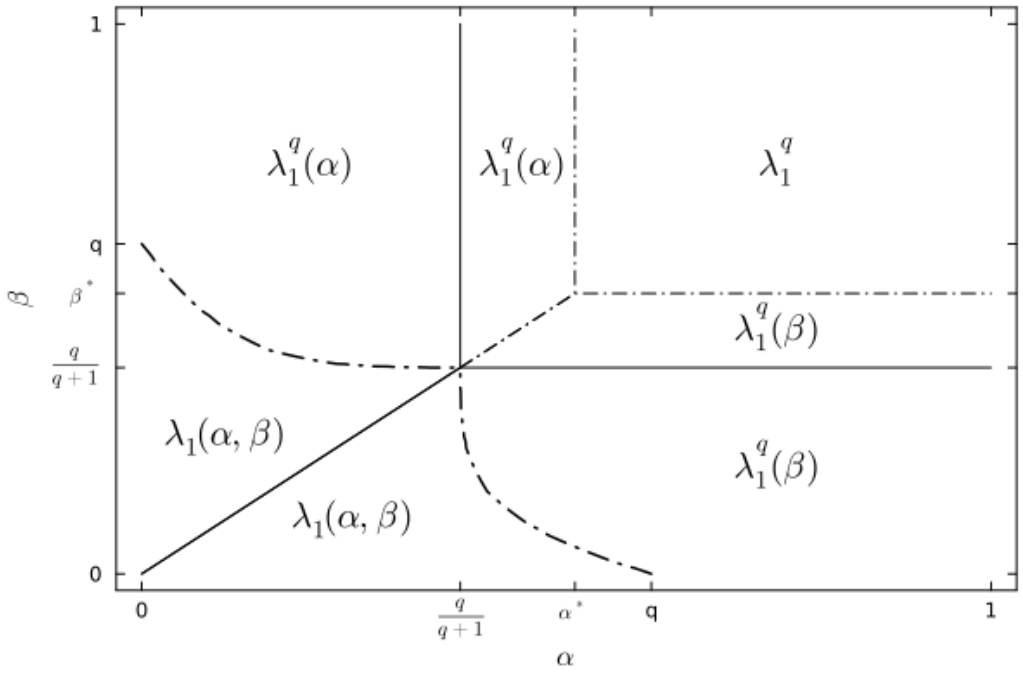

Figure 4.11: Mean-field phase diagram for $h = 1$ depicting all transitions. Static transitions are depicted using solid lines while dynamical transitions are depicted using dash-dotted lines. The position of $\alpha^* = \beta^*$ is illustrative only, numerical results show that α^* and β^* are decreasing functions of q such that for example $\alpha^*(q = 0) = 1$ and $\alpha^*(q = 1) = 1/2$.

Additional results can be found in the Appendix.

As a last comment, let us remind here that all the above results reduce to the pure TASEP ones when $q \to 1$.

[3] Since we consider the thermodynamic limit $L \to \infty$, any dependence on L and k is not made explicit.

4.2 Two-step inhomogeneity ($h = 2$)

Let us briefly consider the case of TASEP with local inhomogeneities of length $h = 2$.

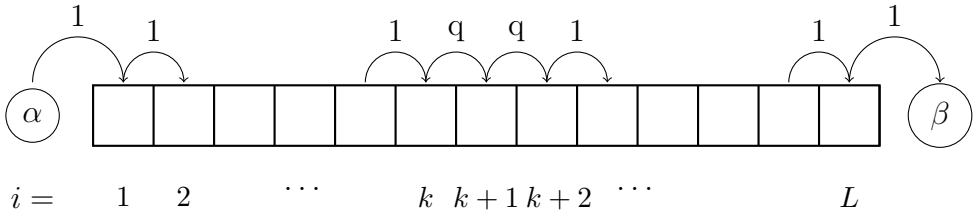

Figure 4.12: Illustration of TASEP with local inhomogeneities of length $h = 2$ with hopping rate q, placed between sites k and $k + 2$.

In this case the continuity equations (2.26) reduce to:

$$\begin{cases} \dot{\rho}_i(t) = \rho_{i-1}(t)(1-\rho_i(t)) - \rho_i(t)(1-\rho_{i+1}(t)), & i \neq k, k+1, k+2 \\ \dot{\rho}_k(t) = \rho_{k-1}(t)(1-\rho_k(t)) - q\rho_k(t)(1-\rho_{k+1}(t)), & \\ \dot{\rho}_{k+1}(t) = q\rho_k(t)(1-\rho_{k+1}(t)) - q\rho_{k+1}(t)(1-\rho_{k+2}(t)), & \\ \dot{\rho}_{k+2}(t) = q\rho_{k+1}(t)(1-\rho_{k+2}(t)) - \rho_{k+2}(t)(1-\rho_{k+3}(t)), & \end{cases} \tag{4.5}$$

with currents (2.27) being

$$\begin{cases} J_i(t) = \rho_i(t)(1-\rho_{i+1}(t)), & i \neq k, k+1 \\ J_i(t) = q\rho_i(t)(1-\rho_{i+1}(t)), & i = k, k+1. \end{cases} \tag{4.6}$$

4.2.1 Stationary states and phase diagram

The above equations, once stationarity is imposed, reduce to:

$$\begin{cases} \rho_{i-1}(1-\rho_i) = \rho_i(1-\rho_{i+1}), & i \neq k, k+2 \\ \rho_{k-1}(1-\rho_k) = q\rho_k(1-\rho_{k+1}), & (i = k) \\ q\rho_{k+1}(1-\rho_{k+2}) = \rho_{k+2}(1-\rho_{k+3}), & (i = k+2) \end{cases} \tag{4.7}$$

which allow us obtain the following:

- for $\alpha < q/2$ and $\alpha < \beta$ the system is in a **low-density (LD)** phase (an example can be seen in Figure 4.13) characterized by bulk density $\rho_{bulk} = \alpha$, stationary current $J = \alpha(1-\alpha)$ and, similar to the case $h = 1$, two boundary layers, one in the proximity of k and one at the end of the lattice; in particular we have specific density values $\rho_{k+2} = \alpha$, $\rho_{k+1} = \alpha/q$ and $\rho_k = \alpha(1-\alpha)/(q-\alpha)$;

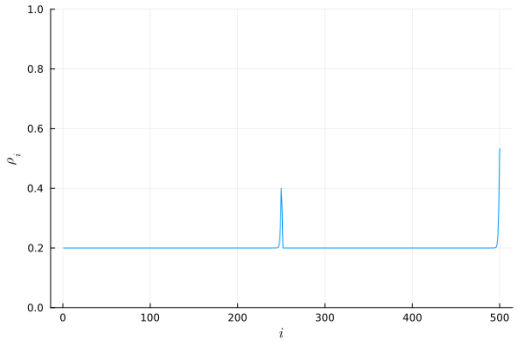

Figure 4.13: Example of mean-field density profile in the LD phase for $h = 2$ ($L = 500$, $\alpha = 0.2$, $\beta = 0.3$, $q = 0.6$).

- for $\beta < q/2$ and $\beta < \alpha$ the system is in a **high-density (HD)** phase (an example can be seen in Figure 4.14) characterized by bulk density $\rho_{bulk} = 1-\beta$, stationary current $J = \beta(1-\beta)$ and two boundary layers, one in the proximity of k and one at the beginning of the lattice; in particular we have specific density values $\rho_k = 1 - \beta$, $\rho_{k+1} = 1 - \beta/q$ and $\rho_{k+2} = 1 - \beta(1 - \beta)/(q - \beta)$;

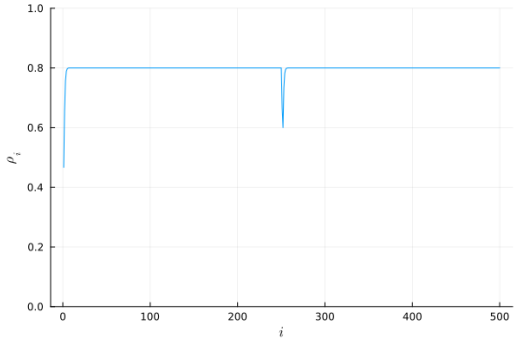

Figure 4.14: Example of mean-field density profile in the HD phase for $h = 2$ ($L = 500$, $\alpha = 0.3$, $\beta = 0.2$, $q = 0.6$).

- for $\alpha, \beta \geq q/2$ the system is in a **maximal current (MC)** phase or **phase separation (PS)** regime (an example can be seen in Figure 4.15) characterized by two bulk densities (similar to the case $h = 1$) $\rho_{bulk,left} = 1 - q/2$ and $\rho_{bulk,right} = q/2$ and two boundary layers; in particular $\rho_k = \rho_{bulk,left}$, $\rho_{k+2} = \rho_{bulk,right}$ and in the middle $\rho_{k+1} = 1/2$;

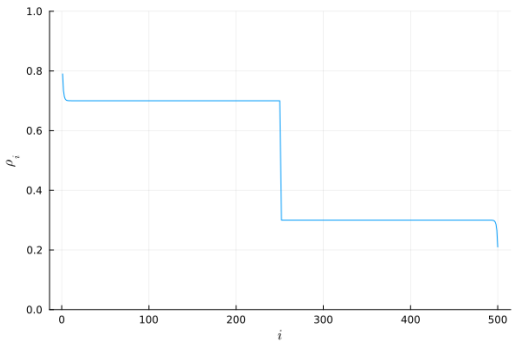

Figure 4.15: Example of mean-field density profile in the PS regime for $h = 2$ ($L = 500$, $\alpha = 1$, $\beta = 1$, $q = 0.6$).

As usual, the above can be schematized in a phase diagram:

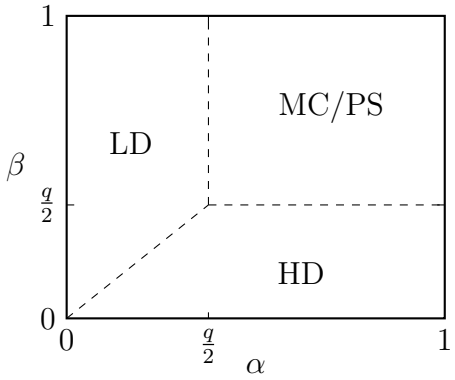

Figure 4.16: Mean-field phase diagram for $h = 2$. Dashed lines denote discontinuous phase transitions.

As seen above, the density profiles in all phases appear to be very similar to the previous case of $h = 1$, apart from details such as the position of transition lines as function of q or the specific values of the densities (e.g. in the two bulks of the PS regime or in the middle layer of the other two phases).

This suggests that the relaxation behavior does not differ greatly from the case of $h = 1$, as we shall see.

4.2.2 Relaxation matrix and dynamical transitions

The symmetrized eigenvalue problem (2.20) takes the form :

$$\begin{cases} M_{i,i}u_i - \sqrt{J}u_{i-1} - \sqrt{J}u_{i+1} = \lambda u_i, & i \neq k, k+1 \\ M_{k,k}u_k - \sqrt{J}u_{k-1} - \sqrt{qJ}u_{k+1} = \lambda u_k, & (i = k) \\ M_{k+1,k+1}u_{k+1} - \sqrt{qJ}u_k - \sqrt{qJ}u_{k+2} = \lambda u_{k+1}, & (i = k+1) \\ M_{k+2,k+2}u_{k+2} - \sqrt{qJ}u_{k+1} - \sqrt{J}u_{k+3} = \lambda u_{k+2}, & (i = k+2) \end{cases} \tag{4.8}$$

with $u_0 = u_{L+1} = 0$.

HD phase: lines of constant β

As one can see in Figure 4.17, also for the case of $h = 2$, the lowest eigenvalue (depicted in blue) shows a threshold behaviour for some $\alpha = \alpha_c(\beta)$ and in Figure 4.18 the HD phase dynamical transition lines (numerically evaluated) are shown.

Also in this case, there is a region of the phase diagram in which the lowest relaxation rate is independent of α; with the lowest rate decreasing with increasing β and going to zero for $\beta = q/2$.

MC/PS phase: lines of constant α

Considering again the lowest rate in the PS phase as a function of β for constant α one finds that the rate is zero for $\beta = q/2$ and non-zero for any $\beta > q/2$; similar to the $h = 1$ TASEP, λ_1 shows a *dynamical transition* in which, for β greater than a threshold value β^*, it reaches a plateau dependent on q.

Numerical evidence suggests the existence of a threshold value q^* (a rough estimate shows $q^* \approx 0.3$) such that for $q > q^*$ the plateau value is the limit $1 - 2\sqrt{J}$, similar to $h = 1$, while for $q < q^*$ it is smaller and the limit value is reached by λ_2 instead. Examples of the two cases are shown in Figure 4.19 (b) and (a), respectively.

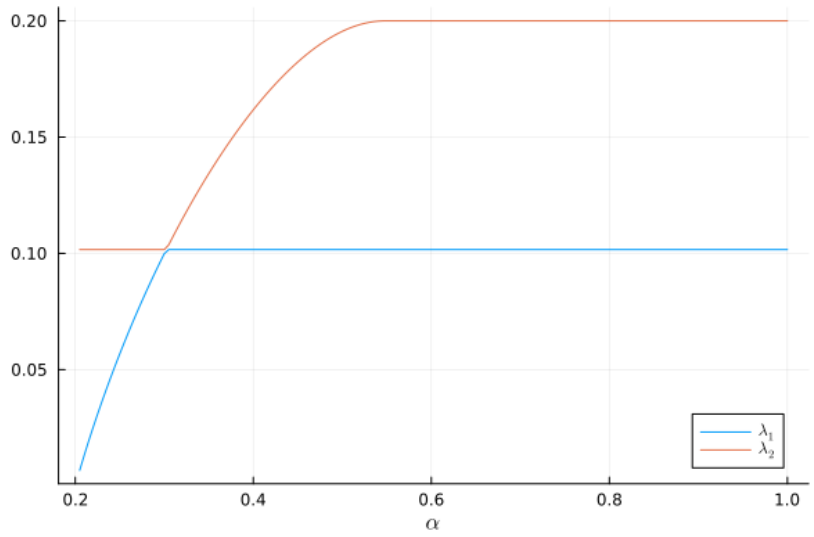

Figure 4.17: The first two lowest eigenvalues as function of α and constant $\beta = 0.2$ ($L = 1000$, $q = 0.6$, $k = 500$). The blue line denotes the lowest rate λ_1, the orange line denotes the second lowest rate λ_2.

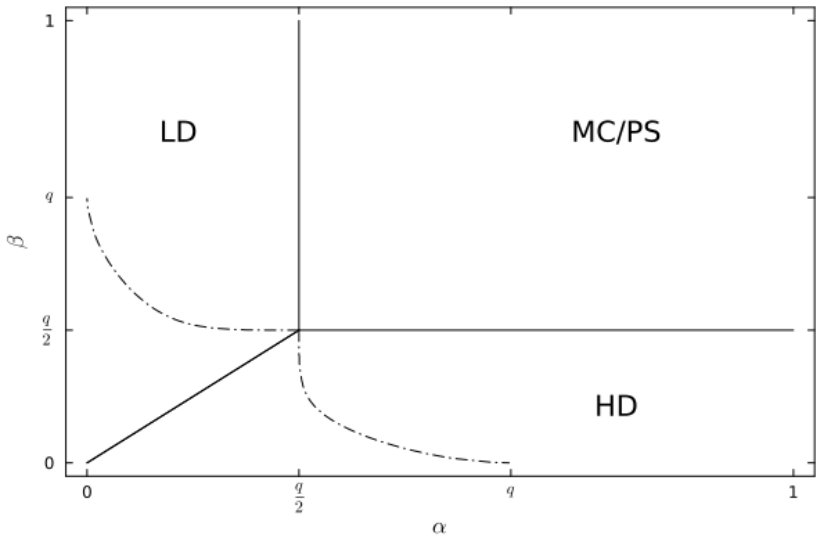

Figure 4.18: Mean-field phase diagram with HD phase dynamical transition lines. Solid lines denote static phase transitions, thin dash-dotted lines denote mean-field (numerical) dynamical transitions.

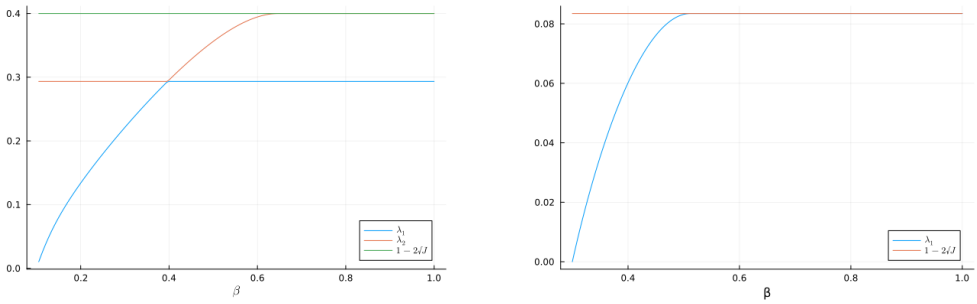

(a) $q < q^*$ (b) $q > q^*$

Figure 4.19: (a) Lowest rates λ_1 and λ_2 as a function of β for $\alpha = 1$ ($L = 1000, q = 0.2, k = 500$), depicted in blue and orange, together with the constant value $1 - 2\sqrt{J}$, for $J = q/2 \cdot (1 - q/2)$, depicted in green.
(b) Lowest rate λ_1 as a function of β for $\alpha = 1$ ($L = 1000, q = 0.6, k = 500$), depicted in blue, together with the constant value $1 - 2\sqrt{J}$, for $J = q/2 \cdot (1 - q/2)$, depicted in orange.

Other considerations done for $h = 1$ also apply here but with the due changes, such as considering $\alpha = \beta = q/2$ as the transition point and noticing that in principle α^*, β^* can be different from the $h = 1$ case, so that the complete behaviour of λ_1 in the PS region can be summarized as follows:

- for $\alpha > \beta$ and $\beta \in (q/2, \beta^*)$ the rate is independent of α,
- for $\beta > \alpha$ and $\alpha \in (q/2, \alpha^*)$ the rate is independent of β,
- for $\alpha \geq \alpha*, \beta \geq \beta^*$ the rate is independent of both boundary rates and only dependent on q.

Using notations similar to the $h = 1$ section (such as $\lambda_1(\alpha, \beta)$ and $\lambda_1^q(\beta)$), the lowest relaxation rate "landscape" can be visualized through a phase diagram, sketched in Figure 4.20, independent of the q^* threshold.

Also for $h = 2$, additional results can be found in the Appendix.

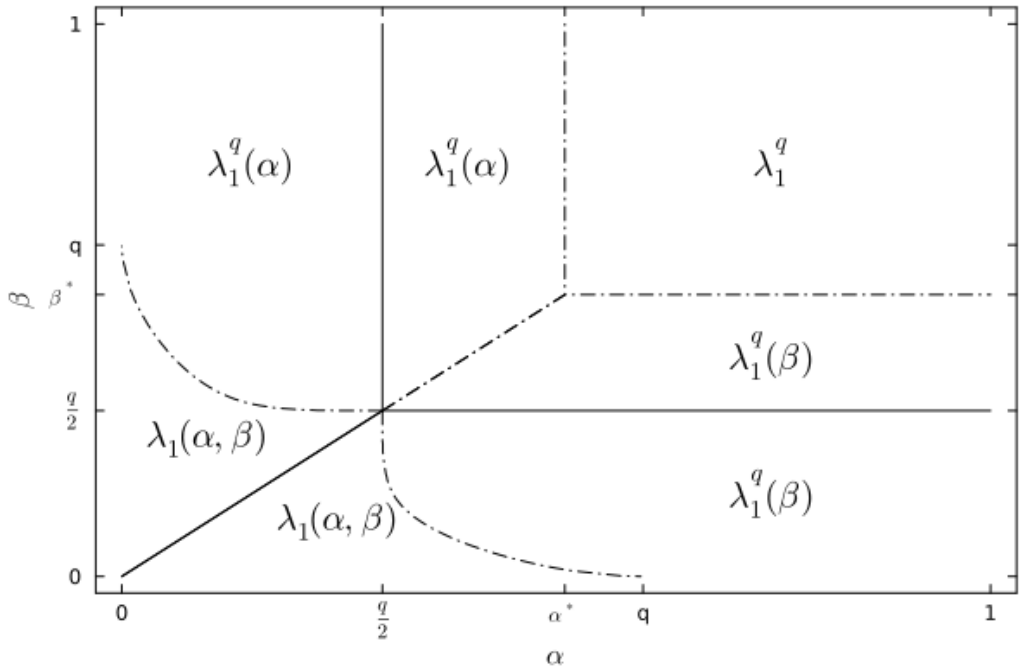

Figure 4.20: Mean-field phase diagram for $h = 2$ displayed all transitions. Static transitions are displayed using solid lines while dynamical transitions are depicted using dash-dotted lines.

Chapter 5

Conclusions

In this work we have investigated the dynamical transitions of the TASEP with local inhomogeneities and, when it was possible, compared it to the pure TASEP dynamical transitions. To do so we applied the mean-field approximation to obtain the non-equilibrium steady states and, most importantly, a simple "framework", through the linearization of the resulting (deterministic) dynamical system, to study the long-time relaxation dynamics of the system.

The main results are the behaviour of the lowest relaxation rate as a function of the injection rate α, the extraction rate β and the value of the inhomogeneity hopping rate q for two specific values of the inhomogeneities region size h. Overall, it shows a richer picture than the one of the pure TASEP, as discussed in the main text, in which the dynamical transitions distinguish between three main different regions of the phase diagram: a "slow" subphase whose dynamical behaviour is determined by both α and β but not by q, a "fast" subphase (which could be further separated into two subphases) governed by the inhomogeneity hopping rate q and only one boundary rate (e.g. β in the HD phase region or α in the LD phase region) and a "boundaries-independent" subphase determined only by q, which is not present in ordinary TASEP, that appears to be a novelty of the TASEP with local inhomogeneities.

Moreover, the transitions can be characterized by the type of the singularities they manifest (through the partial derivatives of the lowest rate with respect to α and β), as done in [7], showing that the "slow" to "fast" subphase transition is *first-order-like*, in contrast to the pure TASEP in which the transition is *second-order-like*, whereas, depending on the parameters h and q, the "fast" to "boundaries-independent" subphase transition can manifest either type of singularity.

In general one can expect that the discussion of the above cases applies also to the general case of TASEP with local inhomogeneities.

In particular, the existence of the three phases low-density, high density and phase separation can easily be argued (see e.g. [8]) whereas, following the present work, one can also expect the relaxation behaviour to show similar dynamical transitions to the ones discussed in this thesis.

However, some details are expected to change, such as the position of the (static and dynamical) transition lines and the functional form of the maximal current, which will depend on the particular value of h.

Appendix

In this Appendix we report some notable cases in which the eigenvalue problem of the relaxation matrix can be analytically studied and, when possible, solved.

Pure TASEP: analytical solution of the eigenvalue problem for $\alpha + \beta = 1$

We consider the special case of a flat density profile, in which $\alpha + \beta = 1$, with stationary current $J = \alpha\beta$. Then, the symmetrized eigenvalue problem reduces to:

$$u_n - \sqrt{J}u_{n-1} - \sqrt{J}u_{n+1} = \lambda u_n \qquad n = 1, \dots, L \tag{1}$$

with boundary conditions $u_0 = u_{L+1} = 0$.

Imposing the ansatz $u_n = x^n$ one reduces the above problem to finding the roots of the characteristic equation, which allows one to write a general solution that then must satisfy the boundary conditions, obtaining the eigenvectors and eigenvalues.

Eigenvalue problem

$$x^n - \sqrt{J}\left(x^{n-1} + x^{n+1}\right) = \lambda x^n, \quad n = 1, \dots, L \tag{2}$$

Characteristic equation

$$x^2 - 2\left(\frac{1-\lambda}{2\sqrt{J}}\right)x + 1 = 0 \tag{3}$$

Roots

$$x_\pm = \left(\frac{1-\lambda}{2\sqrt{J}}\right) \pm \sqrt{\left(\frac{1-\lambda}{2\sqrt{J}}\right)^2 - 1} \tag{4}$$

Eigenvalues

$$\lambda = 1 - \sqrt{J}(x_+ + x_-) \tag{5}$$

General solution

$$u_n = c_+ x_+^n + c_- x_-^n, \quad c_\pm \in \mathbb{R} \tag{6}$$

Boundary conditions
Imposing $u_0 = u_{L+1} = 0$ in the general solution:

$$\begin{cases} c_+ + c_- = 0 \\ c_+ x_+^{L+1} + c_- x_-^{L+1} = 0 \end{cases} \tag{7}$$

Solution Using ϕ as the argument of x_+ (such that $x_+ = e^{i\phi}$)[1], the boundary conditions can be used to obtain the expression of ϕ:

$$\left(\frac{x_+}{x_-}\right)^{L+1} = 1 \implies e^{2i\phi\cdot(L+1)} = 1 \implies \phi = \frac{\pi j}{L+1}, \quad j = 1, \dots, L \tag{8}$$

($j = 0$ would correspond to degenerate roots $x_+ = x_-$ and it can be checked that in this case the boundary conditions cannot be satisfied).

Then it can be used to express both eigenvectors (using $u_1 = c_+(x_+ - x_-)$, instead of c_+) and eigenvalues as a function of ϕ:

$$u_n = u_1 \frac{x_+^n - x_-^n}{x_+ - x_-} = u_1 \frac{e^{in\phi} - e^{-in\phi}}{e^{i\phi} - e^{-i\phi}} = u_1 \frac{\sin(n\phi)}{\sin(\phi)} \propto \sin \frac{\pi n j}{L+1} \tag{9}$$

(by normalization, one can find an explicit value for u_1)

$$\lambda = 1 - 2\sqrt{J}\cos(\phi) \implies \lambda_j = 1 - 2\sqrt{J}\cos\frac{\pi j}{L+1}, \quad j = 1, \dots, L. \tag{10}$$

TASEP with one-step inhomogeneity ($h = 1$): solution of the eigenvalue problem for $\alpha = \beta = 1/(q+1)$

In the case of $\alpha = \beta = 1/(q+1)$, the density profile reduces to a step function with values corresponding to the two bulk densities $\rho_{bulk,left} = 1/(q+1), \rho_{bulk,right} = q/(q+1)$ with stationary current $J = q/(q+1)^2$ (maximal current).

[1] One can easily check that real non-zero solutions cannot exist.

Then, the symmetrized eigenvalue problem reduces to:

$$\begin{cases} u_i - \sqrt{J}u_{i-1} - \sqrt{J}u_{i+1} = \lambda u_i, & i \neq k, k+1 \\ u_k - \sqrt{J}u_{k-1} - \sqrt{qJ}u_{k+1} = \lambda u_k, & (i = k) \\ u_{k+1} - \sqrt{qJ}u_k - \sqrt{J}u_{k+2} = \lambda u_{k+1}, & (i = k+1) \end{cases} \tag{11}$$

with $u_0 = u_{L+1} = 0$.

Using a similar approach to the one in the above section, but adjusting it to take into account that the system is divided into two subsystems, one has:

Characteristic equation

$$x^2 - 2\left(\frac{1-\lambda}{2\sqrt{J}}\right)x + 1 = 0 \tag{12}$$

Roots

$$x_\pm = \left(\frac{1-\lambda}{2\sqrt{J}}\right) \pm \sqrt{\left(\frac{1-\lambda}{2\sqrt{J}}\right)^2 - 1} \tag{13}$$

Eigenvalues

$$\lambda = 1 - \sqrt{J}(x_+ + x_-) \tag{14}$$

General solution

$$u_n = \begin{cases} s_+ x_+^n + s_- x_-^n, & \text{if} \quad n \leq k \\ d_+ x_+^{L+1-n} + d_- x_-^{L+1-n}, & \text{if} \quad n \geq k+1 \end{cases} \tag{15}$$

Boundary conditions

$$\begin{cases} s_+ + s_- = 0 \\ d_+ + d_- = 0 \end{cases} \tag{16}$$

Inhomogeneity conditions

$$\begin{cases} \left(\frac{1-\lambda}{\sqrt{J}}\right)(s_+ x_+^k + s_- x_-^k) & = \sqrt{q}(d_+ x_+^{L-k} + d_- x_-^{L-k}) + (s_+ x_+^{k-1} + s_- x_-^{k-1}) \\ \left(\frac{1-\lambda}{\sqrt{J}}\right)(d_+ x_+^{L-k} + d_- x_-^{L-k}) & = \sqrt{q}(s_+ x_+^k + s_- x_-^k) + (d_+ x_+^{L-k-1} + d_- x_-^{L-k-1}) \end{cases} \tag{17}$$

using the boundary conditions and characteristic equation then

$$\begin{cases} s_+(x_+^{k+1} - x_-^{k+1}) = d_+\sqrt{q}(x_+^{L-k} - x_-^{L-k}) \\ d_+(x_+^{L+1-k} - x_-^{L+1-k}) = \sqrt{q}s_+(x_+^k - x_-^k) \end{cases} \tag{18}$$

$$\Downarrow$$

$$\frac{1}{q} = \frac{x_+^{L-k} - x_-^{L-k}}{x_+^{L+1-k} - x_-^{L+1-k}} \frac{x_+^k - x_-^k}{x_+^{k+1} - x_-^{k+1}} \tag{19}$$

Solution Using ϕ as the argument of x_+ (such that $x_\pm = e^{\pm i\phi}, \phi \in \mathbb{R}$)[2], the inhomogeneity conditions can be used to obtain an equation in ϕ:

$$\frac{1}{q} = \frac{\sin((L-k)\phi)}{\sin((L+1-k)\phi)} \frac{\sin(k\phi)}{\sin((k+1)\phi)} \tag{20}$$

or after some manipulations

$$q = \Big(\cos\phi + \frac{\sin\phi}{\tan(k\phi)}\Big)\Big(\cos\phi + \frac{\sin\phi}{\tan((L-k)\phi)}\Big) \tag{21}$$

which in general must be numerically solved to find all L solutions.

Formally, one can still write that:

$$u_n \propto \begin{cases} \sin(n\phi) & n \leq k, \\ \frac{\sin((k+1)\phi)}{\sqrt{q}\sin((L-k)\phi)} \sin((L+1-n)\phi) & n \geq k+1, \end{cases} \tag{22}$$

with

$$\lambda = 1 - 2\sqrt{J}\cos\phi. \tag{23}$$

In the particular case in which $k = L - k$, the equation in ϕ simplifies and reduces to:

$$q = \Big(\cos\phi + \frac{\sin\phi}{\tan(k\phi)}\Big)^2 \implies \tan(k\phi) = \frac{\sin\phi}{\sqrt{q} - \cos\phi} \tag{24}$$

Then the smallest solution (assuming $\phi \ll \pi$ but such that $\phi \neq 0$) can be obtained by linearizing the terms of the equation (see Figure 1); in particular, we can linearize the tangent term close to its zero $\phi = \pi/k$ (with $k = L/2 \to \infty$), instead we linearize the sine and cosine close to $\phi = 0$:

$$\tan(k\phi) \approx k\phi - \pi, \quad \phi \approx \pi/k \tag{25}$$

$$\frac{\sin\phi}{\sqrt{q} - \cos\phi} \approx \frac{\phi}{\sqrt{q} - 1}, \quad \phi \approx 0 \tag{26}$$

$$\Downarrow$$

[2]One can check that no real exponential solutions exist, i.e. such that $x_\pm = e^{\pm\gamma}, \gamma \in \mathbb{R}$.

$$\phi = \frac{\pi}{k + \frac{1}{1-\sqrt{q}}} = \frac{\pi}{\frac{L}{2} + \frac{1}{1-\sqrt{q}}} \tag{27}$$

which then implies that

$$\lambda_1 \approx 1 - 2\sqrt{J}\cos\frac{\pi}{\frac{L}{2} + \frac{1}{1-\sqrt{q}}} \to 1 - 2\sqrt{J} \tag{28}$$

for $L \to \infty$, as expected.

TASEP with one-step inhomogeneity ($h = 2$): solution of the eigenvalue problem for $\alpha = \beta = 1 - q/2$

Similar to the $h = 1$ case, in the case of $\alpha = \beta = 1 - q/2$, the density profile reduces to a step function with values corresponding to the two bulk densities $\rho_{bulk,left} = 1 - q/2, \rho_{bulk,right} = q/2$, but with $\rho_{k+1} = 1/2$ and stationary current $J = q/2 \cdot (1 - q/2)$ (maximal current).

Then one has:

$$\begin{cases} u_i - \sqrt{J}u_{i-1} - \sqrt{J}u_{i+1} = \lambda u_i, & i \neq k, k+1 \\ u_k - \sqrt{J}u_{k-1} - \sqrt{qJ}u_{k+1} = \lambda u_k, & (i = k) \\ 4Ju_{k+1} - \sqrt{qJ}u_k - \sqrt{qJ}u_{k+2} = \lambda u_{k+1}, & (i = k+1) \\ u_{k+2} - \sqrt{qJ}u_{k+1} - \sqrt{J}u_{k+3} = \lambda u_{k+2}, & (i = k+2) \end{cases} \tag{29}$$

with $u_0 = u_{L+1} = 0$.

Following an approach analogous to that of the previous section, one can obtain:

Characteristic equation

$$x^2 - 2\left(\frac{1-\lambda}{2\sqrt{J}}\right)x + 1 = 0 \tag{30}$$

Roots

$$x_\pm = \left(\frac{1-\lambda}{2\sqrt{J}}\right) \pm \sqrt{\left(\frac{1-\lambda}{2\sqrt{J}}\right)^2 - 1} \tag{31}$$

Eigenvalues

$$\lambda = 1 - \sqrt{J}(x_+ + x_-) \tag{32}$$

General solution

$$u_n = \begin{cases} s_+ x_+^n + s_- x_-^n, & \text{if} \quad n \leq k \\ u_{k+1}, & (n = k+1) \\ d_+ x_+^{L+1-n} + d_- x_-^{L+1-n}, & \text{if} \quad n \geq k+2 \end{cases} \tag{33}$$

Boundary conditions

$$\begin{cases} s_+ + s_- = 0 \\ d_+ + d_- = 0 \end{cases} \tag{34}$$

Inhomogeneities conditions

$$\begin{cases} \sqrt{q} u_{k+1} = \frac{1-\lambda}{\sqrt{J}}(s_+ x_+^k + s_- x_-^k) - (s_+ x_+^{k-1} + s_- x_-^{k-1}) \\ \frac{4J-\lambda}{\sqrt{qJ}} u_{k+1} = (s_+ x_+^k + s_- x_-^k) + (d_+ x_+^{L-k-1} + d_- x_-^{L-k-1}) \\ \sqrt{q} u_{k+1} = \frac{1-\lambda}{\sqrt{J}}(d_+ x_+^{L-k-1} + d_- x_-^{L-k-1}) - (d_+ x_+^{L-k-2} + d_- x_-^{L-k-2}), \end{cases} \tag{35}$$

$$\Downarrow$$

$$\begin{cases} \sqrt{q} u_{k+1} = s_+(x_+^{k+1} - x_-^{k+1}) \\ \frac{4J-\lambda}{\sqrt{qJ}} u_{k+1} = s_+(x_+^k - x_-^k) + d_+(x_+^{L-k-1} - x_-^{L-k-1}) \\ \sqrt{q} u_{k+1} = d_+(x_+^{L-k} - x_-^{L-k}), \end{cases} \tag{36}$$

$$\Downarrow$$

$$\frac{4J-\lambda}{q\sqrt{J}} = \frac{(x_+^k - x_-^k)}{(x_+^{k+1} - x_-^{k+1})} + \frac{(x_+^{L-k-1} - x_-^{L-k-1})}{(x_+^{L-k} - x_-^{L-k})} \tag{37}$$

Solution In terms of ϕ, formally, one can write:

$$u_n \propto \begin{cases} \sin(n\phi) & n \leq k, \\ \frac{1}{\sqrt{q}} \sin((k+1)\phi) & n = k+1, \\ \frac{\sin((k+1)\phi)}{\sin((L-k)\phi)} \sin((L+1-n)\phi) & n \geq k+2, \end{cases} \tag{38}$$

$$\lambda = 1 - 2\sqrt{J}\cos\phi. \tag{39}$$

To find the explicit expression of ϕ one has to impose the inhomogeneity condition:

$$\frac{2\cos\phi}{q} - \frac{1-4J}{q\sqrt{J}} = \frac{\sin(k\phi)}{\sin((k+1)\phi)} + \frac{\sin((L-k-1)\phi)}{\sin((L-k)\phi)} \tag{40}$$

or after some manipulations

$$\frac{1}{Q} - (\frac{1}{q} - 1)\cos\phi = \frac{\sin\phi}{2}\Big(\frac{1}{\tan((k+1)\phi)} + \frac{1}{\tan((L-k)\phi)}\Big), \quad Q \coloneqq \frac{2q\sqrt{J}}{1-4J} \tag{41}$$

which, also in this case, must be numerically solved to find all L solutions.

In the particular case in which $k+1 = L-k$, the equation in ϕ simplifies and reduces to:

$$\frac{1}{Q} - (\frac{1}{q} - 1)\cos\phi = \frac{\sin\phi}{\tan((k+1)\phi)} \implies \tan((k+1)\phi) = \frac{\sin\phi}{\frac{1}{Q} - (\frac{1}{q} - 1)\cos\phi} \tag{42}$$

Then, similarly to the previous section, considering the case in which $\frac{1}{Q} \neq (\frac{1}{q} - 1)$, the smallest solution can be obtained by linearization (see Figure 2), in particular the tangent term is linearized close to $\phi = \pi/(k+1)$ while the sine and cosine are linearized close to $\phi = 0$:

$$\tan((k+1)\phi) \approx (k+1)\phi - \pi, \quad \phi \approx \pi/(k+1), \tag{43}$$

$$\frac{\sin\phi}{\frac{1}{Q} - (\frac{1}{q} - 1)\cos\phi} \approx \frac{\phi}{\frac{1}{Q} - (\frac{1}{q} - 1)} \quad \phi \approx 0, \tag{44}$$

$$\Downarrow$$

$$\phi = \frac{\pi}{k+1+\frac{1}{(\frac{1}{q}-1)-\frac{1}{Q}}} = \frac{\pi}{\frac{L+1}{2}+\frac{1}{(\frac{1}{q}-1)-\frac{1}{Q}}} \tag{45}$$

which then implies that

$$\lambda_1 \approx 1 - 2\sqrt{J}\cos\frac{\pi}{\frac{L+1}{2}+\frac{1}{(\frac{1}{q}-1)-\frac{1}{Q}}} \to 1 - 2\sqrt{J} \tag{46}$$

for $L \to \infty$, again as expected.

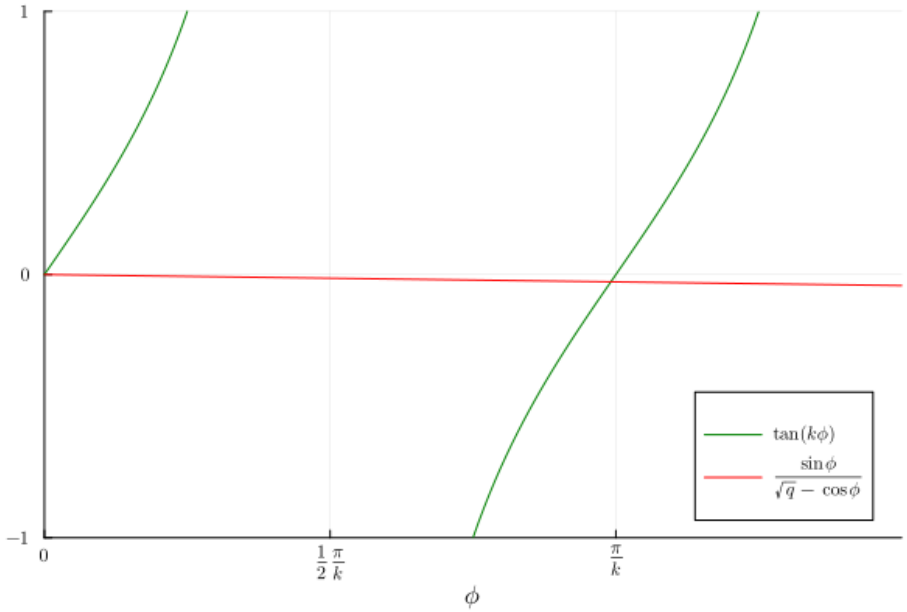

Figure 1: Plot of terms appearing in equation (24). A graphical solution suggests that the first non-zero intersection is close to $\phi = \pi/k$ and motivates the linearization done in the section above.

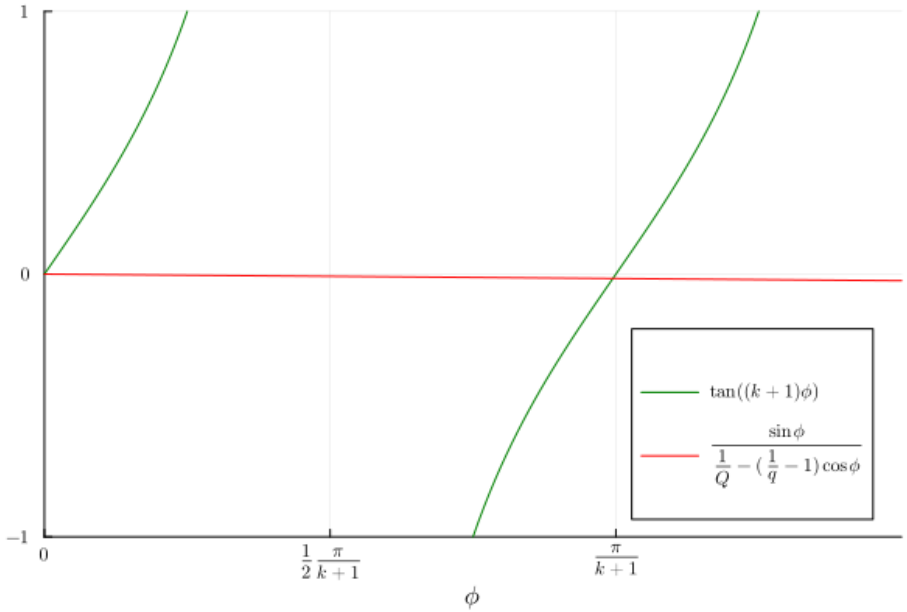

Figure 2: Plot of terms appearing in equation (42). A graphical solution suggests that the first non-zero intersection is close to $\phi = \pi/(k+1)$.

Acknowledgments

I would like to thank all those that supported and guided me through this journey at Politecnico di Torino.

First and foremost, I am grateful to my supervisors Alessandro Pelizzola and Marco Pretti for the guidance they gave throughout the writing of this thesis and most importantly for the opportunity of ending this journey with a rewarding experience.

Then, I would like to acknowledge Politecnico di Torino and the respective Professors for the opportunity to satisfy my academic curiosity through the Master's degree in Physics of Complex Systems, together with my friends here at PoliTo, especially Andrea and Gabriele, with whom I have shared this journey's experiences.

Finally, huge thanks go to my family, who supported me throughout my entire life and encouraged me to follow my passions, and to my friends, both new and old, with whom I have shared many important moments that shaped my life.

Bibliography

[1] A. B. Kolomeisky 1998. Asymmetric simple exclusion model with local inhomogeneity. *J. Phys. A: Math. Gen.*, 31, 1153.

[2] A.Pelizzola and M.Pretti. Cluster approximations for the tasep: stationary state and dynamical transition. *Eur. Phys. J. B*, 90(183), 2017.

[3] K.Nishinari A.Schadschneider, D.Chowdhury. *Stochastic Transport in Complex Systems: From Molecules to Vehicles*. Elsevier, 2010.

[4] D.Mukamel B.Derrida, E.Domany. An exact solution of a one-dimensional asymmetric exclusion model with open boundaries. *J Stat Phys*, 69:667–687, 1992.

[5] A.C. Pipkin C.T. MacDonald, J.H. Gibbs. Kinetics of biopolymerization on nucleic acid templates. *Biopolymers*, 6(1):1–25, 1968.

[6] D. Botto et al 2019. Dynamical transition in the tasep with langmuir kinetics: mean-field theory. *J. Phys. A: Math. Theor.*, 52, 045001.

[7] D. Botto et al 2020. Unbalanced langmuir kinetics affects tasep dynamical transitions: mean-field theory. *J. Phys. A: Math. Theor.*, 53, 345001.

[8] P. Greulich and A. Schadschneider. Phase diagram and edge effects in the asep with bottlenecks. *Physica A: Statistical Mechanics and its Applications*, 387(8):1972–1986, 2008.

[9] F.H.L. Essler J. deGier. Bethe ansatz solution of the asymmetric exclusion process with open boundaries. *Phys. Rev. Lett.*, 95:240601, 2005.

[10] G. Schütz and E. Domany. Phase transitions in an exactly soluble one-dimensional exclusion process. *J Stat Phys*, 72:277–296, 1993.